

2023

# Characterization of mouse models of seasonal coronaviruses to evaluate vaccine efficacy

---

<https://hdl.handle.net/2144/48288>

*"Downloaded from OpenBU. Boston University's institutional repository."*

BOSTON UNIVERSITY

ARAM V. CHOBANIAN & EDWARD AVEDISIAN SCHOOL OF MEDICINE

Thesis

**CHARACTERIZATION OF MOUSE MODELS OF SEASONAL  
CORONAVIRUSES TO EVALUATE VACCINE EFFICACY**

by

**TYLER LEBNER**

B.S., Quinnipiac University, 2021

Submitted in partial fulfillment of the  
requirements for the degree of  
Master of Science

2023

© 2023 by  
TYLER LEBNER  
All rights reserved

Approved by

First Reader

---

Florian Douam, Ph.D.  
Assistant Professor of Microbiology and Investigator, NEIDL

Second Reader

---

Nicholas A. Crossland, D.V.M., DACVP  
Assistant Professor of Pathology and Laboratory Medicine and  
Investigator, NEIDL

Third Reader

---

Elizabeth R. Duffy, M.A.  
Assistant Professor of Pathology and Laboratory Medicine

## **DEDICATION**

I would like to dedicate this work to my wonderful parents and family members who supported me during my graduate education at Boston University's Chobanian and Avedisian School of Medicine. There were countless hours when I would talk aloud whether it be studying for an exam or anything interesting that I was working on in the lab. I appreciate everyone's commitment to providing me with opportunities that I am strongly enthusiastic about.

## **ACKNOWLEDGMENTS**

Florian and Nick, you are truly phenomenal people. Thank you for your wonderful patience and willingness to support me during my graduate academics and research in infectious diseases. I am especially grateful for both of your willingness to guide me in my first lab experience. As mentors, you both have enormously affected me in many ways as a researcher and at a personal level. It has been such a fantastic experience helping you and your teams conduct research in the NEIDL. I am forever grateful to be able to have had this opportunity. This project would also not be complete without the proper and necessary recognition of Giulia Unali, whose virology and molecular biology techniques as well as their patience and their mentorship will be forever appreciated.

Thank you, Aoife O’Connell and Hans Gertje whose guidance in pathology and immunohistochemistry has supported the execution of the work outlined in this thesis.

Truly thank you to the program director, Elizabeth Duffy, and chair of pathology and laboratory medicine, Dr. Christopher Andry for believing in me from the start and for our wonderful conversations during our meetings. Thank you to all the other members of the Douam lab and Crossland lab and to my pathology classmates and MAMS students whom I became friends with during my graduate studies at Boston University.

**CHARACTERIZATION OF MOUSE MODELS OF SEASONAL  
CORONAVIRUSES TO EVALUATE VACCINE EFFICACY**

**TYLER LEBNER**

**ABSTRACT**

**INTRODUCTION:** Seasonal human coronaviruses (HCoV) are endemic to the human population, regularly infecting and reinfecting humans while typically causing asymptomatic to mild respiratory infections. The human coronavirus OC43 (HCoV-OC43) is one of the most common causes of the common cold but can lead to fatal pneumonia in children and the elderly. However, no vaccines or antiviral treatments are available against this virus. Animal models available to study HCoV-OC43 and test antiviral counter measures do not accurately recapitulate the respiratory symptoms and physiopathology observed in humans. These limitations impede our understanding of HCoV-OC43 pathogenesis and the development of efficient antiviral therapies or vaccines.

**Objective:** Animal models are crucial for enhancing our understanding of HCoV-OC43 pathophysiology and pathogenesis, and to enable the development of vaccines or therapeutics. In this study, we tested the susceptibility of various mice models to HCoV-OC43 infection and identified type-I interferon signaling as an immune barrier that restricts HCoV-OC43 infection in mice. Utilizing mice defective for type-I interferon signaling (IFNAR  $-/-$  mice), we established virological and histopathological readouts that could assist in identifying avenues for this model to be used for vaccines and therapeutic evaluations.

**Methods:** C57BL/6, IFNAR<sup>-/-</sup>, and IFNAR<sup>-/-</sup> mice treated with anti-IFN- $\lambda$  (antibodies blocking type-III Interferon cytokines) were infected with different doses of HCoV-OC43. Nasal passages and lung tissues were analyzed at different time points during the course of the infection. Focus forming assay and RT-qPCR were utilized to determine viral titers and loads in the lung, respectively. Tissues were stained with Hematoxylin and eosin for histopathological evaluation and immunohistochemistry was performed for quantification of HCoV-OC43 spike protein via image analysis. Whole slide images were generated using a Vectra Polaris<sup>TM</sup> whole slide scanner and digital analysis with area quantification (AQ) was completed using HALO<sup>TM</sup> v3.5.3.2577 The region of interests included the olfactory and respiratory epithelium of the nasal cavity. Algorithms to quantify the spike protein were designed specifically for each slide. Signal intensity was selected by pixel pigmentation and using the real-time tuning function in HALO<sup>TM</sup> v3.5.3.2577 allowing capture of accurate biological signal. Statistical analysis was conducted using GraphPad Prism<sup>TM</sup> 9.5.1.

**Results:** IFNAR<sup>-/-</sup> mice intranasally inoculated with HCoV-OC43 displayed greater viral antigen in the olfactory epithelium compared to C57BL/6 mice at three-and-five days post infection. IFNAR<sup>-/-</sup> mice also displayed mild histopathological manifestations in the respiratory epithelium compared to infected C57BL/6 wild-type mice. Minor histological characteristics seen in the IFNAR<sup>-/-</sup> mice were characterized by mild rhinitis with neutrophilic and mononuclear influx including edema at the level of the respiratory epithelium, scarce numbers of denuded olfactory epithelium, and mild squamous

metaplasia at the level of the respiratory epithelium. No differences in lung viral loads were observed between the two models throughout the infection course, suggesting that additional immune barriers or absence of specific human factors prevent viral dissemination to the lower respiratory tract in mice. Interestingly, treatment of IFNAR  $-/-$  mice with antibodies targeting type III interferon cytokines increased viral replication in the olfactory epithelium and extended viral dissemination to the respiratory epithelium of the nasal cavity compared to control IFNAR  $-/-$  mice. Altogether, our findings indicate that IFNAR  $-/-$  mice represent a potential mouse model of HCoV-OC43 infection, albeit viral replication is restricted to the nasal cavity. More research is needed to identify additional immune barriers, including type III interferon signaling, restricting viral replication in the mouse respiratory epithelium.

**Conclusion:** Combining virological, molecular biology, and histopathological techniques, our study identify type I and III interferon signaling as restriction mechanisms of HCoV-OC43 replication in the mouse nasal cavity. Our work highlights IFNAR  $-/-$  mice as a potential model to study early HCoV-OC43 pathogenesis, and open avenues for developing advanced mouse models enabling the evaluation of vaccine candidates.

## TABLE OF CONTENTS

DEDICATION .....	iv
ACKNOWLEDGMENTS .....	v
ABSTRACT.....	vi
TABLE OF CONTENTS.....	ix
LIST OF TABLES .....	xii
LIST OF FIGURES .....	xiv
LIST OF ABBREVIATIONS.....	xvi
INTRODUCTION .....	1
Coronavirus Background and Epidemiology.....	1
HCoV-OC43 genomic and protein organization .....	3
Human coronavirus replication and life cycle .....	5
Host cell signaling response triggered by viral entry .....	7
Interferon cytokines responses to viral infections .....	9
Type I interferon response .....	10
Type III interferon response.....	11
HCoV-OC43 pathogenesis .....	12
Coronavirus Vaccines and Therapeutics.....	13
Small animal models for the study of respiratory viruses .....	15
Type-I interferon and STAT1 as an RSV model .....	15
Type-III interferon responses as a model for respiratory viruses .....	16
HCoV-OC43 animal models.....	17

METHODS .....	20
Biosafety .....	20
Cell lines .....	20
HCoV-OC43 and HCoV-NL63 virus stock preparation and titration .....	20
Mice .....	21
Intranasal inoculation with HCoV-OC43 and HCoV-NL63 .....	21
Intranasal treatment with anti-IL28 $\beta$ in IFNAR $-/-$ mice.....	22
Clinical monitoring.....	28
Tissue processing and viral RNA isolation.....	29
Quantification of infectious particles by focus forming assay. ....	29
RNA isolation from serum.....	30
HCoV-OC43 reverse transcription quantitative polymerase chain reaction (RT-qPCR). .....	30
H&E histopathologic evaluation.....	31
Brightfield immunohistochemistry .....	31
Digital whole slide image scanning and analysis of chromogenic immunohistochemistry.....	36
Statistical analysis of brightfield histopathology .....	37
RESULTS .....	38
Depletion of type-I IFN signaling does not increase disease susceptibility to HCoV- OC43 infection in mice.....	38

IFNAR -/- mice display increased pathology in nasal passages upon HCoV-OC43 infection .....	39
Increased HCoV-OC43 replication in the nasal passages of IFNAR -/- mice.....	46
HCoV-OC43 does not effectively replicate in the lung of IFNAR -/- mice.....	53
Approaching the role of type-III IFN in preventing HCoV-OC43 dissemination in the lower respiratory tract.....	55
DISCUSSION .....	59
Mice lacking Type-1 Interferon receptor (IFNAR -/-) display increased susceptibility to HCoV-OC43 infection.....	59
The contribution of type I IFN signaling in restricting HCoV-OC43 infection in mice and governing viral tropism.....	60
The lack of dissemination of HCoV-OC43 in mice suggest the existence of other immunological barriers.....	62
The potential of IFNAR -/- to serve as platform for testing antiviral countermeasures against HCoV-OC43.....	63
Future directions .....	65
BIBLIOGRAPHY.....	67
CURRICULUM VITAE.....	78

## LIST OF TABLES

Table 1. Comparison of various animal models for common respiratory viruses.....	19
Table 2. Study plan 1 for HCoV-OC43 infection in IFNAR $-/-$ and C57BL/6 .....	23
Table 3. Study plan 2 for HCoV-OC43 infection in C57BL/6 wild-type mice only.....	24
Table 4. Study plan 3 for HCoV-OC43 infection in IFNAR $-/-$ mice only. ....	25
Table 5. Study plan 4 for HCoV-OC43 infection in IFNAR $-/-$ mice only with 7 dpi. ....	26
Table 6. Study plan 5 for HCoV-OC43 infection in IFNAR $-/-$ with anti-IFN- $\lambda$ treatment .....	27
Table 7. Clinical scoring criteria.....	28
Table 8. Optimized polyclonal and monoclonal antibodies used for immunohistochemistry.....	33
Table 9. Frequencies of mice challenged with a high dose of $1.00E +6$ FFU of HCoV- OC43 displaying histopathology.....	39
Table 10. Histopathology summary of the nasal passages of IFNAR $-/-$ and C57BL/6 mice infected with different doses of HCoV-OC43. ....	41
Table 11. Frequencies of mice challenged with a high dose of $1.00E+7$ FFU of HCoV- OC43 displaying histopathology in the nasal passages. ....	42

Table 12. Summary of individual histopathology report in 1.00E+7 FFU dose. ....	44
Table 13. Summary of individual histopathology report in 1.00E+7 FFU dose IFNAR -/ only. ....	45
Table. 14. Summary of individual histopathology report in IFNAR -/ mice treated with anti- $\lambda$ . ....	58

## LIST OF FIGURES

Figure 1. Optimized immunohistochemistry protocol for polyclonal antibody detecting HCoV-OC43 spike protein .....	34
Figure 2. Optimized immunohistochemistry protocol for monoclonal antibody detecting HCoV-OC43 spike protein .....	35
Figure 3. Whole slide scan of a full mouse head with annotations.....	36
Figure 4. Visual output of area quantification module in HALO™.....	37
Figure 5. HCoV-OC43 caused no lethal disease in IFNAR- -/- and C57BL/6 wild-type mice.....	38
Figure 6. H&E and anti-Spike staining in the nasal passages of IFNAR -/- and C57BL/6 mice following HCoV-OC43 infection at day 7 post-infection.....	40
Figure 7. H&E and anti-Spike staining in the nasal passages of IFNAR -/- mice following HCoV-OC43 infection (1107 FFU) at day 5 post-infection.....	43
Figure 8. Ordinal scoring of immunohistochemistry targeting HCoV-OC43 spike in the nasal passages of infected C57BL/6 and IFNAR -/- mice.....	46
Figure 9. HCoV-OC43 spike antigen is detectable within the olfactory epithelium .....	47
Figure 10. IFNAR -/- mice show an elevated level of Spike antigens at day 2 post-infection compared to C57BL/6 mice.....	48
Figure 11. Ordinal spike immunoreactivity score in C57BL/6 wild type vs. IFNAR -/- mice.....	49
Figure 12. IFNAR -/- mice show a peak of Spike antigens at day 3 post-infection compared to C57BL/6 mice.....	50

Figure 13. A monoclonal anti-Spike antibody confirms increased susceptibility of IFNAR  
-/- mice to HCoV-OC43 infection. .... 52

Figure 14. Comparison of viral RNA copies and qPCR..... 53

Figure 15. Percent of weight loss between IFNAR -/- treated with anti-IFNλ2, IgG, or  
non-treated upon infection with HCoV-OC43 (10<sup>7</sup> FFU)..... 55

Figure 16. IFNAR -/- mice treated with anti-IFNλ2 are more permissive to HCoV-OC43  
replication in the nasal passages ..... 57

## LIST OF ABBREVIATIONS

ACE2.....	Angiotensin-Converting Enzyme 2
AQ.....	Area quantification
ARDS.....	Acute Respiratory Distress Syndrome
CAP.....	Community-Acquired Pneumonia
CDS.....	Cytosol DNA sensor
BUCASM.....	Boston University Chobanian & Avedisian School of Medicine
BU.....	Boston University
BSL2.....	Biosafety Level 2
CDC.....	Centers for Disease Control and Prevention
CNS.....	Central Nervous System
CoV.....	Coronavirus
COVID-19.....	Coronavirus Disease 2019
DAB.....	Diaminobenzidine
DAD.....	Diffuse Alveolar Damage
DMV.....	Double membrane vesicle
DPI.....	Days Post-infection
ER.....	Endoplasmic reticulum
ERGIC.....	Endoplasmic reticulum-Golgi intermediate compartment
FDA.....	Food and Drug Administration
FFPE.....	Formalin-Fixed Paraffin-Embedded
H&E.....	Hematoxylin & Eosin

hACE2.....	Human Angiotensin-Converting Enzyme 2
HcoV.....	Human coronavirus
HLA.....	Human Leukocyte Antigen
IFITM.....	Interferon-induced transmembrane proteins
IFITM3.....	Interferon-induced transmembrane protein 3
IFNAR -/-.....	Interferon alpha/beta receptor knockout
IFN.....	Interferon
IFNLR.....	Interferon lambda receptor
IFN-λ.....	Interferon lambda
IHC.....	Immunohistochemistry
IRF.....	Interferon-interactive factors
ISG.....	Interferon-stimulating genes
ISGF3.....	Interferon-stimulating gene factor-3
ISRE.....	Interferon-sensitive response element
JAK.....	Janus activated-kinase
mAb.....	Monoclonal antibody
MAVS.....	Mitochondrial antiviral signaling protein
mRNA.....	Messenger RNA
MHC.....	Major histocompatibility complex
MyD88.....	Myeloid differentiation primary response 88
NLR.....	Nod-like receptors
NSP.....	Nonstructural proteins

ORF.....	Open reading frames
PAMP.....	Pathogen-associated molecular pattern
PBMC.....	Peripheral Blood Mononuclear Cells
Poly A.....	Polyadenylation
PRR.....	Pattern recognition receptors
RNA.....	Ribonucleic acid
RBD.....	Receptor binding domain
RdRp.....	RNA-dependent RNA polymerase
RPM.....	Reps Per Minute
RLR.....	Rig-like receptors
RT-qPCR.....	Quantitative Reverse Transcriptase Polymerase Chain Reaction
SOCS1.....	Suppressor of Cytokine Signaling 1
STAT1.....	Signal Transducer and Activator of Transcription 1
TBK1.....	TANK-binding kinase 1
TLR.....	Toll-like receptors
TRAM.....	Signal Transducer and Activator of Transcription
TRAF.....	Tumor necrosis factor receptor-associated factors
TRIF.....	Signal Transducer and Activator of Transcription
TYK2.....	Tyrosine kinase 2

## INTRODUCTION

### **Coronavirus Background and Epidemiology**

Coronaviruses are part of a large group of viruses originating from the order Nidovirales and the family *Coronaviridae* which contain four genera: Alphacoronavirus, Betacoronavirus, Gammacoronavirus, and Deltacoronavirus [1]. Common human coronaviruses are known as the endemic coronaviruses and are referred to as HCoV-OC43, HCoV-229E, HCoV-NL63, or HCoV-HKU1 [2]. These viruses have infections that persist at steady rates in certain geographic regions [3].

The earliest endemic coronaviruses causing common cold-like symptoms were identified in the early 1960s when scientists successfully isolated the first human coronavirus (HCoV, strain B814) from a nasal sample taken from a youth patient with mild upper respiratory tract symptoms [4]. Other coronaviruses such as HCoV-OC43 and HCoV-229E were also isolated and identified in the early to mid-1960s. HCoV-OC43 was presumed to originate from bats, and cattle are known to be intermediate hosts [5],[6]. More recently, other endemic coronaviruses were discovered. In the early 2000s, HCoV-NL63 and HCoV-HKU1 were also identified as endemic coronaviruses that can infect humans and cause disease [7], [8].

These endemic coronaviruses account for nearly 15 - 20% of all seasonal mild upper respiratory tract infections seen globally [9]. HCoV-OC43 infections are heavily associated with direct contact via respiratory droplets and in some cases through fomites. These routes of transmission contribute to the difficulty in preventing the infection spread between humans [10]. Endemic coronaviruses can sometimes result in severe lower

respiratory tract diseases such as pneumonia. These cause hospitalizations, especially in vulnerable populations such as children, immunocompromised individuals, and the elderly [11].

The SARS-CoV-2 pandemic unveiled the global threat posed by coronaviruses [12]. Emerging coronaviruses have the potential to burden communities and result in hospital overflow [13]. In addition, there are currently only four vaccines authorized for emergency use or FDA-approved in the United States to prevent coronavirus infection against SARS-CoV-2. However, despite these vaccines, SARS-CoV-2 infections are still affecting many communities. [14].

HCoV-OC43 and other endemic coronaviruses continue to have a global presence, and this highlights the urgency for endemic coronavirus research to address the threat posed by these viruses. Especially, there is today no vaccines or antiviral drugs against endemic coronaviruses, including HCoV-OC43. Research in endemic coronavirus has been challenged by our limited understanding of viral infection, pathogenesis, and by the lack of suitable *in vivo* models.

HCoV-OC43 and other endemic coronaviruses predominantly infect humans. A cost-effective and small animal model permissive to HCoV-OC43 and recapitulating human disease phenotype is lacking, which has significantly hampered the development of vaccines and therapeutics against HCoV-OC43.

### **HCoV-OC43 genomic and protein organization**

HCoV-OC43 human coronavirus is a single-stranded, positive sense RNA virus harboring an RNA genome of 30,000 nucleotides. Each individual viral transcript has a 5' -cap structure and a 30 poly (A) tail to provide stability during RNA processing [17]. The viral RNA serves as the genome and messenger RNA (mRNA). Upon entry into host cells, the genomic RNA (gRNA) is translated by host cell ribosomes to produce nonstructural proteins (NSPs) from two of the thirteen open reading frames (ORFs), namely ORF1a and ORF1ab, which comprise two-thirds of gRNA sense. The ORF1a is closest to the 5' region and produces polypeptide 1a (pp1a). Directly upstream of the stop codon of ORF1a and before ORF1ab there is a ribosomal frameshift [18]. This is essential for the translation of ORF1ab. Although, this frameshift favors pp1a and results in cleavage of 11 NSP whereas cleavage of pp1ab gives rise to NSP14, NSP15, and NSP16. These cleavages are mediated by cysteine proteases that are found inside NSP3. Additionally, the cleavage of pp1a and pp1ab also are processed into RNA-dependent RNA polymerase (RdRp) encoded from NSP12, which is essential for successful viral transcription and replication [19].

The later of the RNA genome is closest to the 3' end and is transcribed from the sub-genomic mRNA (sgRNA) that encodes for accessory proteins and several structural proteins. Several accessory proteins have been identified and some of these proteins are known to assist the NSP with the replication cycle and evade host immune responses. ORF3a, ORF7a, and ORF7b are some accessory proteins that have functions that can inhibit interferon signaling [20]. It is suggested that ORF3a may have functions that

interfere with the activation of Janus-activated kinase (JAK) by inducing Suppressor of Cytokine Signaling 1 (SOCS1), which results in suppression of interferon (IFN) cytokine production. Additionally, ORF3b was reported to be another antagonist to inhibit IFN production through its C-terminus domain [21].

In addition, the sgRNA also encodes several structural proteins [22]. The four major structural proteins comprise of a nucleocapsid protein (N) and three membrane-associated proteins: envelope glycoprotein, (E), membrane protein (M), and the spike glycoprotein trimer (S) [25]. The (S) protein is a highly glycosylated peplomer crown-like structure extending away from the virus body which binds cell surface host receptors, a critical step for virus entry into host cells[23], [24]. The (S) protein contains three segments comprising of an ectodomain, a single-pass transmembrane anchor, and a short intracellular tail [26]. The ectodomain contains the two functional subunit domains: S1 and S2. The S1 subunit is responsible for attachment via the receptor binding domain (RBD) component and the S2 subunit is responsible for fusion with host cells. Because of the structure of the functioning subunits of the S protein, coronavirus overt the nickname for the “crown”- like structure, which is readily detected by electron microscopy [27]. In HCoV-OC43 infection, the virus utilizes its S protein to attach and enter host cells [28]. Human co-factor such as the 9-0-acyl-sialic acid (9-0-Ac-Sia) binds with the S protein which is then cleaved by furins such as transmembrane proteases like serine-2 (TMPRSS2). HCoV-OC43 virions in fact produce sialate-O-acylesterase protein (HE), that contains an O-acetylated sialic acid-binding domain and sialate O-acylesterase domain that can recognize the human co-factor 9-0-Ac-Sia [29]. Since the entry is

facilitated through the (S) protein, it has resulted in being the main target of antibodies. As a result, the (S) protein is under constant evolutionary pressure and therefore is an important driver of viral evolution [30].

### **Human coronavirus replication and life cycle**

In the early phase of viral entry into host cells, HCoV-OC43 primarily enters through the caveolin-1-dependent pathway of endocytosis. The subunit domains (S1 and S2) will interact and bind to host cell surface molecules such as the 9-O-acetyl-sialic acid (9-O-Ac-Sia), present in many respiratory epithelial cells [4]. In addition to 9-O-Ac-Sia, it is also noteworthy that current literature has potentially recognized additional host factors for HCoV-OC43, such as Interferon-induced transmembrane protein 3 (IFITM3) and the human leukocyte antigen major histocompatibility complex (HLA MHC) class I molecules, although the precise role has yet to be elucidated.

IFITM3 is part of the IFITM family, which is heavily associated with antiviral functions [31]. Induced transmembrane proteins (IFITM) predominantly reside in the plasma membrane and in many cases, function by preventing viral adhesion by the viral membrane and the host's membrane [32]. These proteins are important as they not only assist in antiviral response but play important roles in viral pathogenesis. On the contrary, it is known that HCoV-OC43 infection is enhanced via the interaction with IFITM3. This interaction also acts to facilitate fusion into host cells [33]. Importantly, single nucleotide changes of IFITM (polymorphism) define different levels of disease severity

upon infection by several common respiratory viruses, including the human coronavirus HCoV-OC43 [34].

HLA is a family of proteins that regulate immune responses [35]. HLA are critical mediators of adaptive immune responses and of an individual's ability to fight specific aggressions. In the context of HCoV-OC43 infections, HCoV-OC43 can interact with HLA MHC class I molecules on the surface of host cells to facilitate fusion. MHC class I is present on all nucleated somatic cells whereas MHC class II is largely restricted to antigen-presenting cells or professional antigen-presenting cells as dendritic cells. MHC Class I molecules present endogenous peptides to CD8<sup>+</sup> T- cells [36]. Specifically, the MHC class I- $\alpha$ 2 chain is one potential factor that allows cleavage of the S1 and S2 domains. In addition, previous in-vitro experiments provide ample evidence that HCoV-OC43 has a strong binding affinity to HLA MHC class I and serves as an additional co-factor for entry and viral infection in humans [37]. [38].

Some of the NSP develop into the replicase-transcriptase complex (RTC), such as NSP2-NSP16. These proteins assemble to promote optimal conditions for RNA replication and transcription of the sub-genomic RNAs [39]. NSP3, NSP4, and NSP6 contribute to RNA replication by promoting the development of cellular microenvironments defined by DMV (double membrane vesicle) formation, CMs (convoluted membranes), and DMSs (double membrane spherules). By generating a replication intermediate (negative-stranded RNA), the viral RNA replication process will produce de novo genomic and sg RNAs, with the sgRNA serving as templates for translation of the structural and accessory proteins [40]. Following translation, structural proteins are inserted into the

endoplasmic reticulum (ER) where the proteins finally reach the endoplasmic reticulum-Golgi intermediate compartment (ERGIC) and are encapsulated by the N protein enabling viral particle assembly [41]. As newly synthesized progeny are produced, virions are released primarily through budding by the mechanism of exocytosis. Once released from the infected cell, virions can infect other neighboring cells/or new hosts through respiratory droplets and aerosols.

### **Host cell signaling response triggered by viral entry**

The innate immune response comprises of some of the initial responses towards microbial pathogens. This response utilizes pattern recognition receptors (PRR), which can detect molecular structures on pathogens known as pathogen-associated molecular patterns (PAMPs) [42]. PAMPs are conserved molecular motifs that are associated with the invading pathogen. Examples of PAMPs include nucleic acids such as dsRNA, DNA, ssRNA, and lipopolysaccharides [43]. These PRR consist of RIG-I-like receptors (RLR), toll-like receptors (TLR), and Nod-like receptors (NLR) [44]. TLR can also be found at the plasma membrane to recognize extracellular PAMPs [31]. They can also be present and detect an assortment of nucleic acids from the internalization or processing of pathogens inside endosomes [45]. TLR-7 and TLR-8 are examples of TLR present in the endosome and can recognize single-stranded RNA (ssRNA). While in the cytosol, NLR, RIG-I, and Cytosolic DNA sensors (CDS) can recognize bacterial cell walls, viral RNA, and microbial DNA. Protein adapters such as Myeloid differentiation primary response 88 (MyD88), (TLR domain-containing adapter protein) TRIF, and TRIF-related adaptor

molecule (TRAM) are required for the innate immune signaling of TLR to proceed with the activation and regulation of the transcription factors NF- $\kappa$ B and the IRF complexes in addition to the MAPK signaling pathways [46].

RLR is a group of RNA sensors that are crucial in viral infections, as they mediate the transcriptional factor of host antiviral genes to produce cytokines such as type-I interferon. Examples of RLR include RIG-I, melanoma differentiation-associated protein 5 (MDA5), and laboratory of genetics and physiology 2 (LGP2) [47]. The structure of all RLR have a centralized helicase domain and a carboxy-terminal domain (CTD) and have primary functions to detect and stimulate a response towards viral RNA [48]. In addition, RLR are also localized to the cytosol and are effective at recognizing RNA viruses containing 5' triphosphate (5'-ppp). As RIG-I recognizes the 5'-ppp of viruses such as HCoV-OC43 this results in the activation and recruitment of an adapter molecule known as mitochondrial antiviral signaling protein (MAVS). Once activated MAVS mediates downstream signaling of two pathways, tumor necrosis factor receptor-associated factors 6 (TRAF6) and tumor necrosis factor receptor-associated factors 3 (TRAF3). TRAF6 pathway results in the activation of NF- $\kappa$ B. The TRAF3 pathway leads to activating the TANK-binding kinase 1 (TBK1) complex, leading to the phosphorylation and dimerization of the interferon-interacting factors (IRF) IRF3 and IRF-7 [49]. Both NF- $\kappa$ B and IRF3/7 can translocate to the nucleus to activate/promote the production of type-I interferon cytokines.

## **Interferon cytokines responses to viral infections**

Interferons are secreted cytokines that are produced when cells are infected with a virus and undergoing stress. Interferon cytokines can activate host defense mechanisms to inhibit further viral infection and viral replication. The binding of type-I interferon to the interferon  $\alpha/\beta$  receptor (IFNAR) at the cell surface of infected and bystander uninfected neighboring cells initiates the JAK/STAT pathway leading to the transcription of interferon stimulating genes (ISG). As a result, an antiviral response is induced to help prevent further viral replication or de novo infection

In addition to RIG-I signaling to produce interferon cytokines, TLR-7 and TLR-8 also assist with interferon signaling and production. As the virus enters the cytosol and the ssRNA genome is released, through autophagy or receptor-mediated endocytosis, the ssRNA genome can enter the endosome. TLR-7 and TLR-8 can then interact with the ssRNA to induce signal transduction. In relation to RIG-I, TLR-7, and TLR-8 also signals through TRAF3 and TRAF6 to promote IRF7 which as stated above leads to the production of type-I interferons [50], [51].

As described above, interferon cytokines can be produced by cells that are infected with either intracellular or extracellular pathogens [52]. There are several different cytokines that virally infected cells can produce in an attempt to stimulate a response. Examples of some cytokines include type-I interferons, type-II interferons, and type-III interferons. As a result, there are several different interferon ligand-binding receptors and pathways for their respective cytokines. In addition, interferon responses also provide a linkage to the adaptive immune response by activating professional antigen-presenting cells such as

dendritic cells (DC). In an innate immune response plasmacytoid DC (pDC) are known as “professional IFN- $\alpha/\beta$ ” and contain few PRR that can recognize viral nucleic acid and produce cytokines in response to numerous viruses.

pDC also expresses TLR7 and has a high expression of IRF-7 [53]. In particular, they can produce high levels of type-I interferons when TLR7 interacts with viral RNA. pDC can be found in various compartments in the body such as the thymus, lymph nodes, spleen, and Peyers patches which can contribute to the enhancement of antigen presentation. Upon pDC processing and presentation of viral RNA, they present the antigen to T lymphocytes [54]. As a result of providing strong antigen presentation, this additionally enhances the antiviral functions of other immune cells such as monocytes, B-cells, and natural killer cells (NK) [55], [56], [57].

#### *Type I interferon response*

The type-I interferon signaling initiates with interferon cytokines, produced by virally infected cells, binding to their respective ligand. In a type-I interferon response, these cytokines bind to cell surface receptors known as IFNAR1 and IFNAR2 [58], [59].

Inside the cytosol, IFNAR1 is associated with a tyrosine kinase 2 (TYK2) and IFNAR2 is associated with a Janus activating kinase 1 (JAK1) protein. In a physiological response, the IFN  $\alpha/\beta$  binding to IFNAR1 and IFNAR2 ligand initiates IFNAR1 and IFNAR2 heterodimerization and the phosphorylation of JAK1 and TYK2. This allows for the phosphorylation of STAT1 and STAT2 which forms a complex with IRF9 known as interferon-stimulated gene factor-3 (ISGF3). ISGF3 then translocates into the nucleus and binds to interferon-stimulatory responsive elements (ISREs), resulting in ISG

transcription and translation. Type-1 interferon can also induce activation of proinflammatory transcription factors and genes [60].

### *Type III interferon response*

Type-III interferon (IFN- $\lambda$  or Interleukin-28) response signaling occurs through IL28R $\alpha$  and IL10R $\beta$  with the outcome activating proinflammatory genes similarly to the type-1 interferon alternative signaling pathway. There have been four type-III interferons identified; IFN- $\lambda$ 1 (IL-29), IFN- $\lambda$ 2 (IL-28A), IFN- $\lambda$ 3 (IL-28B), and IFN- $\lambda$ 4 and all are encoding on the 19<sup>th</sup> chromosome of the human genome [61], [62]. Type-III interferon interactions with IL28R $\alpha$  and IL10R $\beta$  initiates the receptor heterodimerization and the phosphorylation of JAK1 and TYK2. This leads to the phosphorylation of STAT1 and STAT2. While type I and III interferon signaling employ similar signaling pathways to drive antiviral responses, they induce a different pattern of ISG upon infection [64]. The molecular mechanisms behind these differences remain poorly understood [65].

However, it is recognized that unlike type I IFN signaling, JAK2 contributes to type III IFN signaling and is necessary for STAT1 phosphorylation [66].

A key feature of type III IFN signaling is the specific tissue distribution of the type III IFN receptors and the preferential ability of this antiviral mechanism to protect the epithelial barrier and induce localized antiviral responses, unlike type I IFN which are more systemic and inflammatory. Indeed, type III IFN signaling is critical in mediating antiviral responses in the respiratory epithelium and other surface barriers such as the gastrointestinal mucosa, the skin, or the vagina [67]. IFN- $\lambda$  cytokine has been shown in

the literature to be a protective response in vitro and in vivo against many respiratory viruses such as norovirus, cytomegalovirus (CMV), rotavirus, and coronaviruses [68].

### **HCoV-OC43 pathogenesis**

Before notable outbreaks and pandemics were caused by coronaviruses, HCoV-OC43 was one of the few *Coronaviridae* that was known to be pathogenic in humans [69].

HCoV-OC43 can cause a variety of symptoms ranging from mild upper respiratory tract illnesses to severe histopathology and inflammation of the lower respiratory tract.

Common symptoms include a headache, runny nose, fever, and sore throat. In younger populations, elderly, and immunocompromised individuals, infections often are more severe and cause bronchitis, pneumonia, and even death [70]. HCoV-OC43 and the endemic coronaviruses predominantly replicate in the upper respiratory tract in epithelial cells, whereas SARS-CoV-2 can more extensively disseminate to the lower respiratory tract and lungs. Unlike SARS-CoV-2, endemic coronaviruses are not known to cause acute respiratory distress syndrome (ARDS) and diffuse alveolar damage (DAD) [71]. HCoV-OC43 can also invade the central nervous system (CNS) [72].

As the virus enters host cells, infection triggers a cell-intrinsic response that can recruit an assortment of immune cells such as dendritic cells and macrophages to the site of infection. Cellular infiltration, along with antigen presentation by infected cells and by subsequent infiltrated cells, initiates local inflammation aimed at protecting the tissues from further viral spread. While inflammation is associated with rhinitis and nasal congestion, dysregulation of such response can drive a more severe disease.

S is also an important driver of HCoV-OC43 pathogenesis. As a major determinant of virus entry and target of host-mediated neutralizing responses, S antigenic divergence over time can drive immune evasion and/or alter cellular tropism; which can significantly impact the course of infection and/or disease. [73].

### **Coronavirus Vaccines and Therapeutics**

There are currently no other vaccines or treatments available for coronaviruses other than SARS-CoV-2. Vaccines are crucial for communities to assist with preventing the spread of illnesses, particularly, respiratory viruses. Recent advances in vaccine development over the past few decades, including mRNA vaccines, have uniquely positioned us to devise effective vaccines against coronaviruses, as demonstrated by the vaccines against SARS-CoV-2,[74],[75],[76]. The first-ever vaccines developed for coronaviruses were in light of the SARS-CoV-2 (COVID-19) pandemic [77]. Notably, the vaccines developed for the SARS-CoV-2 target the (S) protein. When the mRNA is released into the cytosol of cells, ribosomes will translate and produce the (S) protein. When the immune system recognizes the spike protein, this triggers an adaptive immune response that produces antibodies against S, allowing it to block virus entry if the virus is encountered.

Vaccination against SARS-CoV-2 has been instrumental in reducing hospitalization and severe disease[75]. In the United States, there are currently four U.S. Food and Drug Administration (FDA) approved vaccines and several other vaccines that are authorized for emergency use. Two of the FDA-approved vaccines are mRNA-based (Pfizer BioNTech and Moderna NIAID). The third vaccine is a viral vector (Johnson and

Johnson's Janssen) and the fourth vaccine is a subunit protein vaccine (Novavax) [4],[78],[79]. [80]. However, S-based vaccines present limitations as they can be outpaced overtime by S antigenic divergence and the emergence of novel variants, requiring constant vaccine updates. [80].

An important limitation of current vaccine approaches against coronavirus also involves their inability to prevent infection and community spread. For this reason, researchers have been identifying alternative coronavirus vaccines strategies such as live attenuated vaccines, inactivated vaccines, and subunit vaccines [81]. While a live attenuated vaccine can produce a more robust immune response there are potential risks associated. This includes the potential of reversion to the fully virulent form and the suboptimal suitability of live vaccines for vulnerable populations such as immunocompromised and elderly individuals [82]. Unlike the current vaccination route which uses intramuscular injection, the development of mucosal vaccine strategies -using current or novel vectorization methods (mRNA and subunit vaccine)- is now heavily considered as the right path forward to increase the ability of coronavirus vaccine to protect from infection. The knowledge gained from the development of SARS-CoV-2 vaccines can help guide vaccine development for endemic coronaviruses. It is likely that the development and evaluation of vaccine strategies against SARS-CoV-2 will benefit the design of effective vaccines against endemic coronaviruses such as HCoV-OC43.

### **Small animal models for the study of respiratory viruses**

Due to the widespread distribution of endemic human coronaviruses, there is an urgent need for research surrounding these viruses. Researchers have faced barriers attempting to study the endemic coronaviruses [83]. Viruses such as the HCoV-OC43 have a narrow species tropism and not all animals such as laboratory mice are susceptible to infection. Mouse represents a cost-effective and highly convenient animal model to study viruses, evaluate vaccines, and understand antiviral immune responses. However, conventional do not recapitulate the human infection or disease course of many human coronaviruses, including HCoV-OC43. For HCoV-OC43 specifically, infection of current mouse models either results in neurotropism, lack of human manifestations of disease and or are not permissive to viral infections [84]. One hypothesis for the inability of conventional mice to support infection and/or recapitulate human disease is that they mount different antiviral responses compared to humans which makes them refractory to infection. Alternatively, they may also lack certain viral co-factors that are essential for human coronavirus infection of human host cells. Altogether, this underscores the inability of current mouse models to serve as a platform to develop and evaluate vaccines against HCoV-OC43. This exemplifies the need for developing novel mouse models of HCoV-OC43 infection.

#### *Type-I interferon and STAT1 as an RSV model*

Mice defective for the expression of IFNAR (IFNAR  $-/-$ ) are readily used in research to investigate the contributions of the type I IFN signaling pathways during viral infection or other disease context. The Respiratory Syncytial Virus (RSV) is another common

respiratory virus widespread across human populations, and similarly to HCoV-OC43, it can cause severe lower respiratory tract disease in children and immunocompromised individuals [85]. Mice defective for STAT1 expression are more susceptible to RSV infection. IFNAR  $-/-$  mice challenged with RSV are also more permissive to viral replication in the nasal passages compared to wild-type mice but did not display an increasing susceptibility to infection to the same extent as STAT1  $-/-$  mice, suggesting that defect in type-III IFN signaling through STAT knock-out may increase infection susceptibility.[86].

*Type-III interferon responses as a model for respiratory viruses*

In addition to designing animal models utilizing IFNAR  $-/-$  mice, type-III IFN has also been leveraged to develop models of influenza. In literature, it is suggested that type-III IFN assists in antiviral responses against respiratory viruses such as influenza. The role of this cytokine pathway has been contemplated for instance in transgenic mice models overexpressing Mx1. Mx1 is a gene known as the influenza resistance gene. Mx1 and GTPase and are heavily studied in influenza research [87],[88]. Induced by type-I and type-III IFN, this GTPase is highly associated with innate immune responses toward viral infections. The function of MX1 is primarily to inhibit the viral replication of influenza [89]. Mx1-overexpressing mice infected with influenza strains and treated with IFN- $\lambda$  intranasally were more extensively protected from severe lung disease compared to those not treated with IFN- $\lambda$  [90], [91].

*HCoV-OC43 animal models*

In literature, few animal models have been developed to study endemic human coronaviruses. BALB/c mice inoculated intracerebrally with HCoV-OC43 exhibited severe disease and viral neurotropism. Severe disease was characterized by detrimental effects on the central nervous system (CNS) including encephalitis and neuronal degeneration, which led to low survival rates. Hippocampal changes were also observed. However, the inability of BALB/c mice to recapitulate respiratory tract infection is a severe limitation. This model also falls short to provide clinically relevant readouts that could serve vaccine evaluations (see table 1) [93]. Alternatively, HCoV-OC43 animal models relying on intracranial inoculation of suckling C57BL/6 wild-type mice mount severe disease phenotype and show viral neurotropism. While this model relies on a mouse-adapted strain harboring mutations in S, it still carries the same limitation as the BALB/c model (absence of respiratory tract infection and disease) also making it unsuitable for vaccine evaluation. The goal of this study is to establish a novel mouse model for HCoV-OC43 infection that recapitulates human disease. C57BL/6 mice were challenged intranasally with HCoV-OC43 and displayed low permissiveness to viral infection and did not recapitulate a human disease phenotype. These results ultimately provided directions to explore models with increased susceptibility to HCoV-OC43 infections, which could ultimately serve as platforms for vaccines and antiviral drug evaluations.

IFNAR<sup>-/-</sup> mice are partially immune deficient. Dr. Edward E. Schmidt, Montana State University, developed the IFNAR<sup>-/-</sup> mice model by breeding IFNAR1<sup>fl</sup> mice with

SOX2-Cre mice and then removing the SOX-Cre alleles resulting in the creation of mice lacking expression of IFNAR1. [95]. While this mouse model retains the functionality of many arms of the immune system, it displays enhanced permissiveness to viral infection (96). Despite ample evidence for this mouse model to be more permissive to many viral infections, the susceptibility of IFNAR  $-/-$  mice to HCoV-OC43 infection is unknown [97].

In this work, we hypothesize that mice defective for type I and/or type III IFN signaling could potentially be more permissive to HCoV-OC43 infection. IFNAR  $-/-$  mice were evaluated through classical molecular, virological, and pathological approaches with the goal to identify a novel mouse model of HCoV-OC43 infection and pathogenesis.

Especially, we aim to identify whether such a model recapitulates infection of the respiratory tract as observed in humans, and can potentially serve as a platform for the evaluation of vaccines and therapeutics

Mouse Model	Delivery of Infection	Infectious agents	Clinical manifestation	Advantages	Disadvantages
BALB/c	intracerebrally	HCoV-OC43	High rates of mortality, neurological deficits,	Successful viral replication	Neurotropism
Suckling C57BL/6	intracerebrally	HCoV-OC43	Significant loss in body weight In pups	Pneumonia and lower respiratory tract disease	Mouse adapted strain of HCoV-OC43 (HCoV-OC43 VR-1588 P.9)
IFNAR -/- and IFNAR-λ	Intranasal	Influenza A	No treatment - weight loss and pneumonia seen 7 + 9 dpi	IFN-λ treatment enhanced innate immune response in IFNAR -/-	Intranasal treatment with IFN-λ protected mice from severe disease
IFNAR -/- STAT1 -/-	Intranasal	RSV	Mild upper respiratory tract symptoms	Full innate immune competence	Possible of negative feedback by ERK ubiquitination
hAPN+/+ Stat-/- and hAPN-/- Stat+/+	Intranasal	HCoV-229E	Mild weight loss, elevated temperatures	Successfully viral replication in the lung	Double transgenic mice, deficient in innate immune responses
K18-hACE2	Intranasal	HCoV-NL63, HCoV-229E SARS-CoV-2	Mild to moderate severe disease, pneumonia	Successful viral replication	Neurotropism

**Table 1. Comparison of various animal models for common respiratory viruses and endemic human coronavirus HCoV-OC43.**

## METHODS

### **Biosafety**

All aspects of this study were approved by the Institutional Biosafety Committee and the office of Environmental health and Safety at Boston University prior to study initiation. All work with HCoV-OC43, in vivo and in vitro, was performed in an animal biosafety level-2 (ABSL2) laboratory or biosafety level-2 (BSL2) by qualified personnel equipped with appropriate personal protection equipment (PPE). Following euthanasia and necropsy in the ABLS2, all remaining work was done in a biosafety level-2 (BSL2) laboratory. Tissues were either stored in RNAlater to preserve viral load for quantification or chemically inactivated for a minimum of 72 hours before being processed for histopathology.

### **Cell lines**

The Rhabdomyosarcoma (RD), CACO2, THP1, and (PBMCs) were maintained in Dulbecco's Modified Eagle Medium (DMEM) containing 10% fetal bovine serum (FBS, ThermoFisher Scientific, Waltham, MA, USA), 1% penicillin and streptomycin, and incubated at 37 degrees Celsius and 5% CO<sub>2</sub> humidified incubator.

### **HCoV-OC43 and HCoV-NL63 virus stock preparation and titration**

HCoV-OC43 strains of coronavirus were kindly provided from industry partners (Moderna Inc.) Viruses were propagating on rhabdomyosarcoma cells (RD cells) for HCoV-OC43.

## **Mice**

Mice were maintained in a facility accredited by the Association for the Assessment and Accreditation of Laboratory Animal Care (AAALAC). Animal protocols were approved by Boston University Institutional Animal Care and Use Committee. Homozygous IFNAR  $-/-$  mice of both sexes were obtained from the Jackson Laboratory (Jax, Bar Harbor, ME) and bred in the laboratory. For breeding, homozygous IFNAR  $-/-$  mice male and female were paired. Mice were housed at the Animal Science Core (ASC, 670 Albany Street, Boston, MA) before being transferred over to the National Emerging Infectious Diseases Laboratories (NEIDL) for experiments. Animals were grouped together based on sex and kept in ventilated cages prior to and during experiments.

## **Intranasal inoculation with HCoV-OC43 and HCoV-NL63**

At 5 –15 weeks of age, IFNAR  $-/-$  and wild type C57BL/6 mice of both sexes were intranasally inoculated with either a low dose of  $1.00E+4$  FFU, a high dose of  $1.00E+6$  FFU, and an increased dose of  $1.00E+7$  FFU of HCoV-OC43 in  $50\mu\text{L}$  of sterile 1 x PBS (n=117 [n=60 male and n=57' female], or sham inoculated with  $50\mu\text{L}$  of sterile 1 x PBS (n=4; 2 male, 2 female). Mice were euthanized at the designated endpoints of either 2- or 7-days post-infection (low and high dose) or 1-, 3-, 5-, and 7-days post-infection for  $1.00E+7$  FFU. Decalcified whole heads were grossed accordingly and sagittal sections of the nasal turbinates were processed for histopathology. Blood was collected from the heart and serum was separated. In addition, the lungs were also collected. Nasal turbinates from the animals were stored in a 50mL Falcone tube with 10% neutral buffered formalin (NFB). Blood was collected in a 2mL Eppendorf tube. Upon collection

of the blood samples, they were immediately centrifuged for 10 minutes at 13,000 rpm and plasma from the blood samples was extracted. E Each bronchiole of the lungs was separated and placed into 1.5mL tubes containing 600 $\mu$ l of RNA Later to allow for subsequent viral quantification via FFA and qPCR.

### **Intranasal treatment with anti-IL28 $\beta$ in IFNAR -/- mice**

IFNAR -/- mice of both sexes were either treated intranasally with a recombinant mouse anti-IL28 $\beta$  (Cat # mil28b-mab9-1, Invitrogen) (n=5) or IgG1 (n=5), 1 day prior to infection and 8 ours post-infection. Included in this cohort were mice infected but with no antibody treatment (n=3) and mice that were uninfected and had no antibody treatment. HCoV-OC43 viral stocks were generated by propagating the virus in RD cells, and the viral titer obtain was  $3.6 \times 10^8$  FFU/mL. The virus was administered intranasally in mice in 50 $\mu$ L of sterile 1 x PBS (see previous infections above). Three days post-infection, all mice were euthanized, and organs were harvested to observe and determine key factors that assisted or prevented infection or disease.

*OC43; 48 mice; 2 mouse strains; 2 endpoints; 2 viral doses*

<b>2022-OC43-C1</b>		
	<b>Variables</b>	
<b>Settings</b>	Nber/Strain	24 BL6 and 24 IFNARKO
	Virus	OC43
	Dose	<b>1e4 and 1e6 FFU</b>
	Route	intranasal
<b>Experimental groups</b>	6 C57BL/6 1e4 FFU	2DPI endpoint
	6 C57BL/6 1e4 FFU	7DPI endpoint
	6 C57BL/6 1e6 FFU	2DPI endpoint
	6 C57BL/6 1e6 FFU	7DPI endpoint
	6 IFNARKO 1e4 FFU	2DPI endpoint
	6 IFNARKO 1e4 FFU	7DPI endpoint
	6 IFNARKO 1e6 FFU	2DPI endpoint
	6 IFNARKO 1e6 FFU	7DPI endpoint
<b>EndPoint</b>	2DPI	qPCR/FFU on lung tissue, histopathology and OC43 Spike IHC evaluation in nasal passage, serum collection
	7DPI	qPCR/FFU on lung tissue, histopathology and OC43 Spike IHC evaluation in nasal passage, serum collection

**Table 2. Study plan for HCoV-OC43 infection in IFNAR -/- and C57BL/6**

Viral doses for infection include a low dose,  $1.00E + 4$ , and a medium dose,  $1.00E + 6$  FFU, with endpoints of 2- and 7-days post-infection.

*OC43; 21 mice; 1 mouse strain; 5 endpoints; 1 viral dose*

2022-OC43-C1-Level 2		
Date of infection	07/19/2022	
	Variables	
Settings	Nber/Strain	21 BL6
	Virus	OC43
	Dose	1e7 FFU
	Route	intranasal
Experimental groups	4 C57BL/6 1e7 FFU	1DPI endpoint
	4 C57BL/6 1e7 FFU	2DPI endpoint
	4 C57BL/6 1e7 FFU	3DPI endpoint
	4 C57BL/6 1e7 FFU	5DPI endpoint
	4 C57BL/6 1e7 FFU	7DPI endpoint
	1 C57/BL6 uninfected FFU	1 DPI endpoint
EndPoint	1DPI	qPCR/FFU on lung tissue, histopathology and OC43 Spike IHC evaluation in nasal passage, serum collection
	2DPI	qPCR/FFU on lung tissue, histopathology and OC43 Spike IHC evaluation in nasal passage, serum collection
	3DPI	qPCR/FFU on lung tissue, histopathology and OC43 Spike IHC evaluation in nasal passage, serum collection
	5DPI	qPCR/FFU on lung tissue, histopathology and OC43 Spike IHC evaluation in nasal passage, serum collection
	7DPI	qPCR/FFU on lung tissue, histopathology and OC43 Spike IHC evaluation in nasal passage, serum collection

**Table 3. Study plan for HCoV-OC43 infection in C57BL/6 wild-type mice only.**

Mice were inoculated with  $1.00E + 7$  FFU and euthanized at either 1, 2, 3, 5, or 7, days post-infection.

*OC43; 13 mice; 1 mouse strain; 3 endpoints; 1 viral dose*

<b>2022-OC43-C2-Level 2 (Moderna)</b>		
<b>Date of infection</b>	<b>08/18/2022</b>	
	<b>Variables</b>	
<b>Settings</b>	Nber/Strain	13 IFNARKO
	Virus	OC43
	Dose	<b>1e7 FFU</b>
	Route	intranasal
<b>Experimental groups</b>	4 IFNARKO 1e7 FFU	1DPI endpoint
	4 IFNARKO 1e7 FFU	3DPI endpoint
	4 IFNARKO 1e7 FFU	5DPI endpoint
	1 IFNARKO uninfected FFU	1 DPI endpoint
<b>EndPoint</b>	1DPI	qPCR/FFU on lung tissue, histopathology and OC43 Spike IHC evaluation in nasal passage, serum collection
	3DPI	qPCR/FFU on lung tissue, histopathology and OC43 Spike IHC evaluation in nasal passage, serum collection
	5DPI	qPCR/FFU on lung tissue, histopathology and OC43 Spike IHC evaluation in nasal passage, serum collection

**Table 4. study plan for HCoV-OC43 infection in IFNAR -/- mice only.**

Mice were inoculated with  $1.00E + 7$  FFU and euthanized at either 1, 3, or 5, days post-infection

OC43; 22 mice; 1 mouse strain; 3 endpoints; 1 viral dose

2022-OC43-C3-Level 2 (Moderna)		
Date of infection	12/08/2022	
	Variables	
Settings	Nber/Strain	22 IFNARKO
	Virus	OC43
	Dose	1e7 FFU
	Route	intranasal
Experimental groups	7 IFNARKO 1e7 FFU	3DPI endpoint
	7 IFNARKO 1e7 FFU	5DPI endpoint
	7 IFNARKO 1e7 FFU	7DPI endpoint
	1 IFNARKO uninfected FFU	1 DPI endpoint
Endpoint	3DPI	qPCR/FFU on nasal washes and lung tissue, histopathology and OC43 Spike IHC evaluation in nasal passage and lungs serum collection
	5DPI	qPCR/FFU on nasal washes and lung tissue, histopathology and OC43 Spike IHC evaluation in nasal passage and lungs, serum collection
	7DPI	qPCR/FFU on nasal washes and lung tissue, histopathology and OC43 Spike IHC evaluation in nasal passage and lungs, serum collection
Schedule	12/12/22	3DPI endpoint
	12/13/22	5DPI endpoint
	12/15/22	7DPI endpoint

**Table 5. study plan for HCoV-OC43 infection in IFNAR -/- mice only.**

Mice were inoculated with  $1.00E + 7$  FFU and euthanized at either 3, 5, or 7, days post-infection

<b>2022-OC43-C4-anti-IgG1 and anti-IFN<math>\lambda</math> treatment (Moderna)</b>		
<b>Date of infection</b>	<b>03/03/2023</b>	
	<b>Variables</b>	
<b>Settings</b>	Nber/Strain	IFNAR-KO
	Virus	HCoV-OC43
	Dose	<b>1e7 FFU</b>
	Route	intranasal
<b>Experimental groups</b>	3 IFNAR KO (no treatment), infected	3 DPI endpoint
	5 IFNAR-KO (treatment with IgG1) OC43 1e7 FFU	3DPI endpoint
	5 IFNAR-KO (treatment with anti-IFN $\lambda$ ) OC43 1e7 FFU	3DPI endpoint
	1 IFNAR KO control (no treatment, non infected)	-
<b>Endpoints</b>	3DPI	H&E and IHC on all nasal passages, qPCR lung tissue, H&E and IHC on partial lung., serum collection
<b>Schedule</b>	Treatment with anti-IgG1	3/2/2023
	Treatment with anti-IFN $\lambda$	3/2/2023
	Mice infected with HCoV-OC43	3/3/2023
	3/6/2023	3DPI endpoint

**Table 6. study plan for HCoV-OC43 infection in IFNAR -/- with anti-IFN- $\lambda$  treatment**

## Clinical monitoring

Animals included in the low and high-dose infection were checked daily and on the day of the takedown. Additionally, animals included in the low and high dose (n = 48, sham = 0) were intraperitoneally implanted with an RFID temperature-monitoring microchip (Unified Information Devices, Lake Villa, IL, USA) 48-72 hours prior to inoculation. An IACUC-approved clinical scoring system was utilized to monitor disease progression and establish humane endpoints (**Table 7**). Categories evaluated included body weight, general appearance, responsiveness, respiration, and neurological signs for a maximum score of 5. Animals that were considered moribund were humanely euthanized in the event of the following: a score of 4 or greater for 2 consecutive observation periods, weight loss greater than or equal to 20%, severe respiratory distress, or lack of responsiveness.

Category	Score = Criteria
Body weight	1 = 10-19% loss
Respiration	1 = rapid, shallow, increased effort
Appearance	1 = ruffled fur, hunched posture
Responsiveness	1 = low to moderate unresponsiveness
Neurological signs	1 = tremors

**Table 7. Clinical scoring criteria**

This scoring system was used for clinical monitoring of HCoV-OC43-infected IFNAR<sup>-/-</sup> and wild type C57BL/6 mice.

**Tissue processing and viral RNA isolation**

Tissues were collected from mice and placed in tubes containing 600 $\mu$ L of RNAlater (Sigma-Aldrich; # R0901500ML) and stored at -80 °C. For processing of lung tissues, 30 – 75 mg of tissue were weighted on a high precision balance scale and placed into a 2 mL Eppendorf tube with 600 $\mu$ L of RLT buffer and a 5 mm stainless steel bead (Qiagen, Valencia, CA). Tissues were homogenized using a Qiagen TissueLyser II (Qiagen; Germantown, MD) by two dissociations cycles (two-minutes at 1,800 oscillations/minute) with a one-minute rest in between. Samples were centrifuged at 17,000 X g (13,000 rpm) for 10 minutes and supernatant was transferred to a new 1.5 ml tube. Viral RNA isolation was performed using a Qiagen RNeasy Plus Mini Kit (Qiagen), according to the manufacturer's instructions. RNA was finally eluted in 50 $\mu$ L of RNase/DNase-free water and stored at -80 °C until used.

**Quantification of infectious particles by focus forming assay.**

Quantification of OC43 infectious particles were performed by focus forming assay (FFA). After euthanizing mice, tissues were collected in 600  $\mu$ L of RNAlater (ThermoFisher Scientific) and stored at - 80 °C until used. One day prior to the experiments, a 96-well plate containing  $3.0 \times 10^4$  cell/well of RD cells in DMEM, 10% fetal bovine serum (FBS), and 1% HEPES were plated. Virus (HCoV-OC43) was diluted in 50 $\mu$ L and placed into each well for the infection and the 96-well plate was incubated at 37°C for 1 hour. 150 $\mu$ L of 1500cP (high viscosity) methylcellulose (MEM, 2% FBS, 1% HEPES) was then added to each well and the plate was incubated for 26 hours. For staining after incubation, the methylcellulose layer was carefully removed and 200 $\mu$ L of

4% PFA/PBS (paraformaldehyde solution Cat #15713-S) was added and incubated for 15 minutes at room temperature. PFA was removed and disposed of appropriately. The plate was washed with 100 $\mu$ L solution containing .1% tritone, .1% BSA in PBS. 50 $\mu$ L of primary antibody targeting HCoV-OC43 nucleocapsid protein (rabbit IgG polyclonal, Sino Biological, Cat # 40643-T62, 1:6000) was then added and incubated for 2 hours at room temperature. 100 $\mu$ L of ELISA wash (PBSTween 0.005%) was then added. A secondary antibody (goat anti-rabbit-HRP, 1:1000) was then applied and incubated for 45 minutes at room temperature. 100 $\mu$ L of ELISA was then added and 60 $\mu$ L of TrueBlue HRP (KPL TrueBlue peroxidase substrate, SeraCare, Cat # 5510-0030) was added for and protected from light for 15 minutes. Finally, the 96-well plate was washed with distilled water and set to dry. Foci were then counted using a light source. Viral titers can be determined by counting the number of foci present in each well of the 96-well plate.

### **RNA isolation from serum.**

Upon collection of the blood samples from a heart puncture procedure, they were immediately centrifuged for 10 minutes at 13,000 rpm and plasma from the blood samples were extracted and transferred to a new 1.5mL Eppendorf tube and stored at -80°C until used.

### **HCoV-OC43 reverse transcription quantitative polymerase chain reaction (RT-qPCR).**

Viral RNA was isolated using Qiagen RNeasy Plus Mini Kit (Qiagen) as described above. A standard curve was developed with a serial dilution of known standard curve RNA. A master mix containing primers (10 $\mu$ M of forward and 10 $\mu$ M of reverse) were

mixed with LOW ROX 2X solution, and a 10uM probe, all targeting HCoV-OC43 was used in order to perform RT-qPCR. RT-qPCR was performed using an Applied Biosystems QuantStudio (ThermoFisher Scientific) and the following cycling conditions: reverse transcription for 10 minutes at 55 degrees Celsius, an activation step at 95 degrees Celsius for 3 minutes followed by 45 cycles of denaturation at 94 degrees Celsius for 15 seconds combined annealing/extension at 58 degrees Celsius for 30 seconds. For each sample, QuantStudio™ Design and Analysis Software v1.3.1 (ThermoFisher Scientific) provided an amplification curve constructed by relating the fluorescence signal intensity to the cycle number.

### **H&E histopathologic evaluation**

5µm sections were prepared from FFPE (formalin-fixed, paraffin-embedded) decalcified whole heads and insufflated whole lungs, and transferred to positively charged glass slides. Tissue samples were deparaffinized and stained with hematoxylin and eosin (H&E) using a combined Leica Autostainer-coverslipper unit ST5010-CV5030 (Leica Microsystems, Wetzlar, Germany). Slides were qualitatively analyzed by Dr. Nicholas Crossland, a board-certified veterinary pathologist, in order to determine key pathological features within the tissue (see table below).

### **Brightfield immunohistochemistry**

Immunohistochemistry (IHC) was performed using a Ventana BenchMark Discovery Ultra Autostainer (Roche Diagnostics, Indianapolis, IN, USA). OC43 spike (S) protein was semiquantitatively scored as follows: 0, no immunoreactivity observed; 1, rare single cell immunoreactivity; 2, multifocal small sporadic aggregates of immunoreactive cells.

Antigen retrieval was conducted using a Citrate based buffer-Cell Conditioning 2 (CC2). The HCoV-OC43 spike antibodies were rabbit derived and thus required a secondary goat derived anti- rabbit antibody HRP-polymer (Vector Labs, Burlingame, CA). Brightfield slides were then exposed to a DAB (3,3' Diaminobenzidine) kit to form a brown precipitate in proximity to primary and secondary antibody complexes that contained the HRP conjugate. Slides were then counterstained with hematoxylin, dehydrated, and cleared using a combined Leica Autostainer-coverslipper unit ST5010-CV5030 (Leica Microsystems, Wetzlar, Germany). Coverslips were applied and slides were set aside to dry before observing under the microscope. Polyclonal and monoclonal antibodies from the same manufacture were compared. Changes from the polyclonal antibody to the monoclonal antibody include the removal of primary heat incubation and the addition of a pre-primary protein block with shortened antigen retrieval. **Table 8** highlights the details of each antibody. **Figure 1 and figure 2** highlight the optimized protocols used for staining with the polyclonal and monoclonal antibodies specific for the spike protein of HCoV-OC43.

<b><u>Antibody</u></b>	Polyclonal	Monoclonal
<b><u>Manufacture</u></b>	Cell Signaling Technologies	Cell Signaling Technologies
<b><u>Clone</u></b>	N/A	MWP10017-1
<b><u>Species derived</u></b>	Rabbit	Rabbit
<b><u>Pretreatment</u></b>	CC2-91°C	CC2-91°C
<b><u>Duration</u></b>	32 min	24 min
<b><u>Primary antibody dilution</u></b>	1:100	1:600
<b><u>Incubation duration</u></b>	40 min	32 min

**Table 8. Optimized polyclonal and monoclonal antibodies used for immunohistochemistry staining**

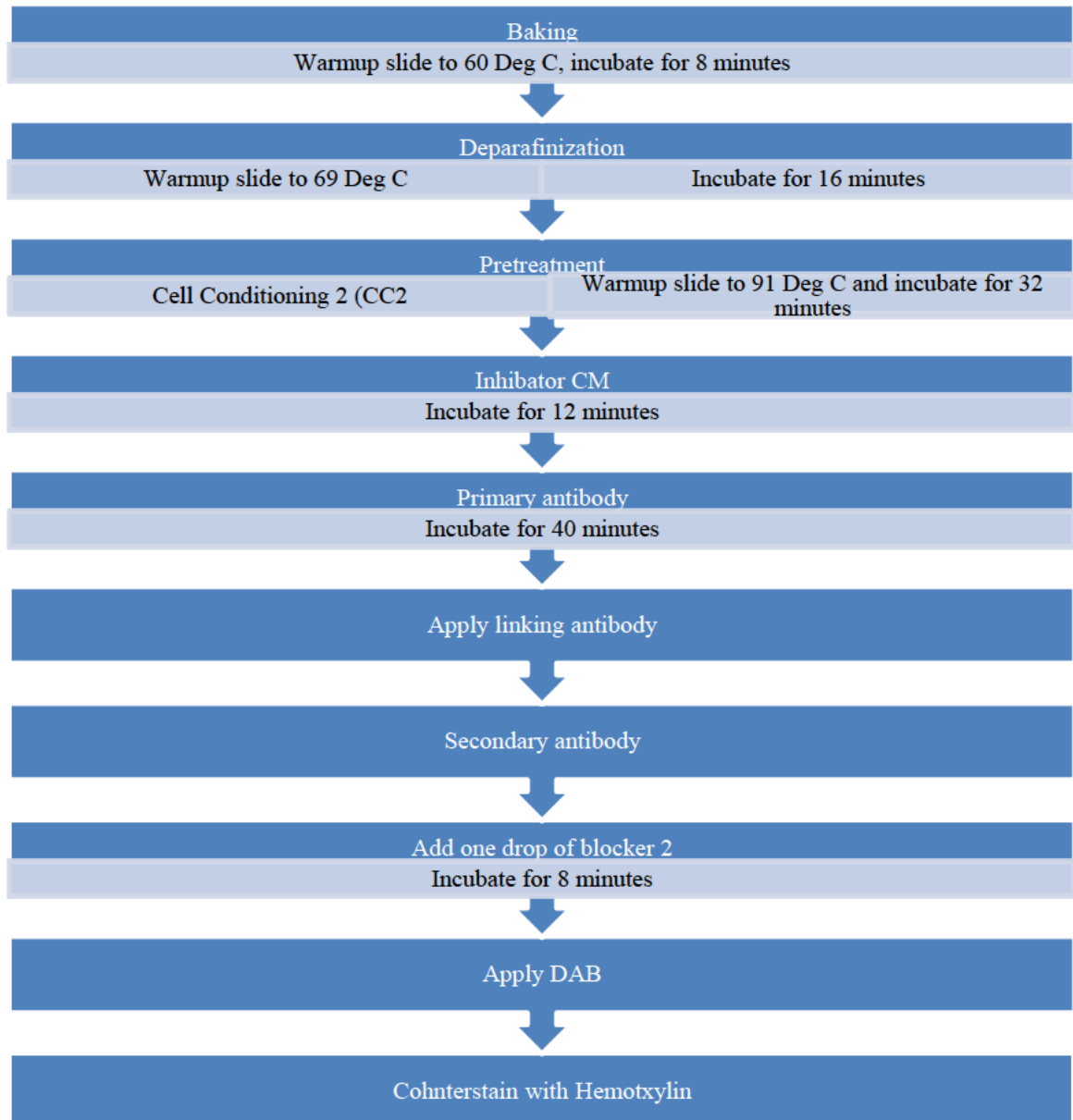


**Figure 1. Optimized immunohistochemistry protocol for polyclonal antibody detecting HCoV-OC43 spike protein**

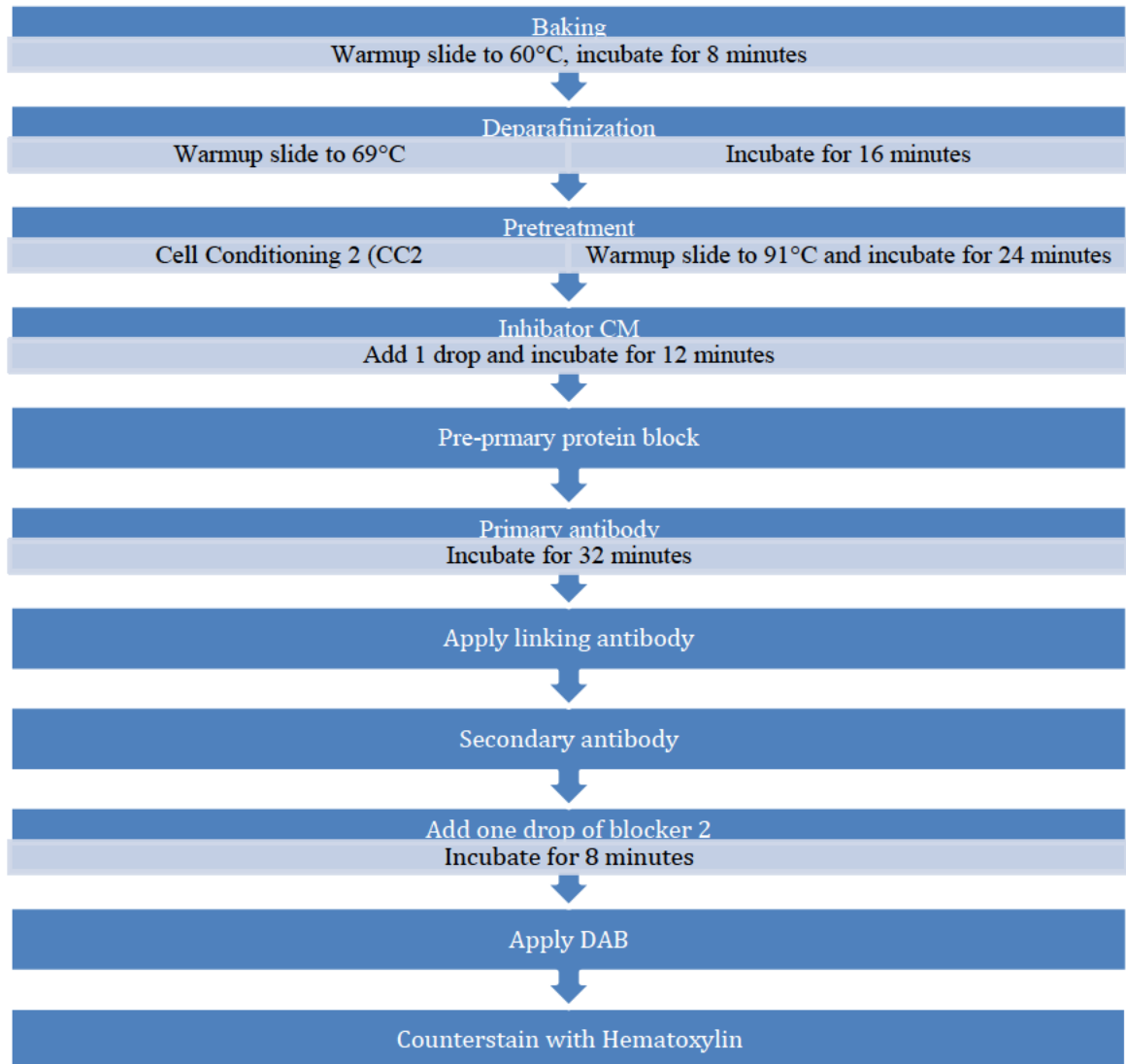


**Figure 2. Optimized immunohistochemistry protocol for monoclonal antibody detecting HCoV-OC43 spike protein**

## **Digital whole slide image scanning and analysis of chromogenic immunohistochemistry**

Chromogenic immunohistochemistry labeled slides were imaged using a Vectra Polaris Quantitative Pathology Imaging System (Akoya Biosciences). H&E slides and immunohistochemistry slides were scanned using a 20x brightfield protocol. Immunohistochemistry images and files were then transferred to HALO™ (Indica Labs, Inc., Corrales, NM). A midline sagittal section of a mouse head with the olfactory epithelium annotated for image analysis (**Figure 3**).

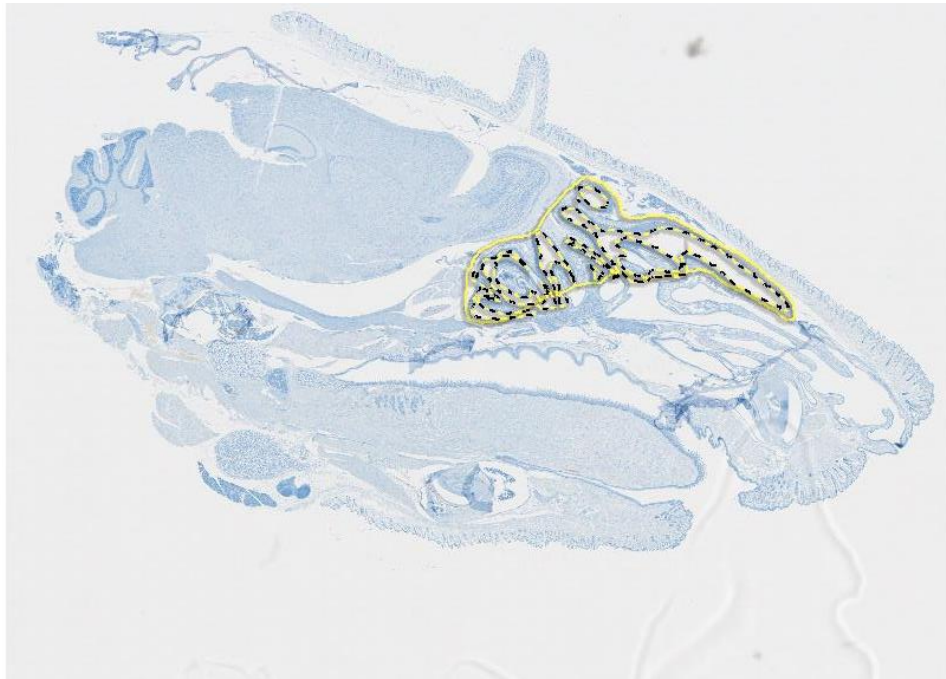


**Figure 3. Whole slide scan of a full mouse head with annotations**

Representative image from uninfected C57BL/6 wild-type mice. The solid yellow line represents the olfactory epithelium (to be analyzed), whereas the dashed yellow line denotes areas within the olfactory epithelium to be excluded from the analysis.

### Statistical analysis of brightfield histopathology

Descriptive statistics and graphics were performed using GraphPad Prism V9.5.1 statistical analysis software (GraphPad, Sand Diego, CA). Total percent of pixels were captured for  $1.00E+4$ ,  $1.00E+6$ , and  $1.00E+7$  FFU and were utilized to accurately capture HCoV-OC43 viral spike protein and signal of the Immunohistochemistry. Quantitative pathology results were analyzed using either Mann-Whitney independent t-test and one-way or two-way ANOVA to determine the presence of statistical significance between each group. Tukey's multiple comparison tests were used to determine the differences between groups.

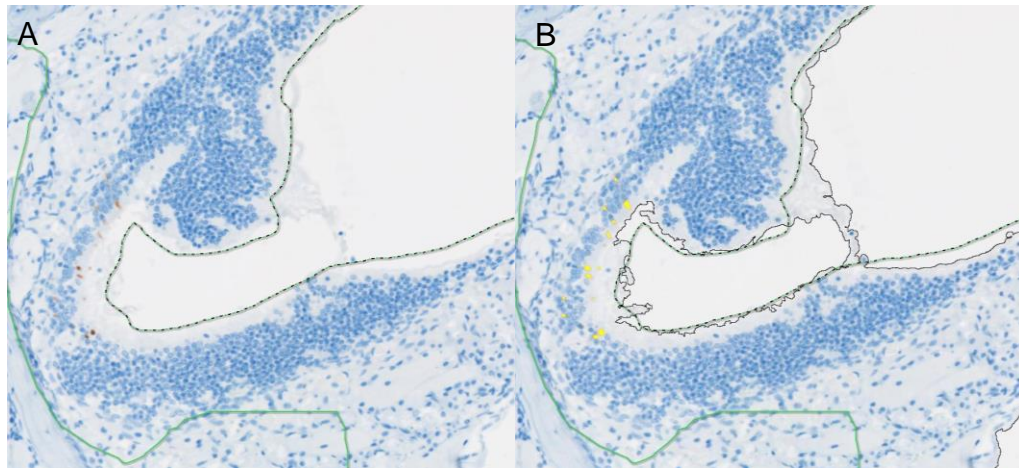


**Figure 4. Visual output of area quantification module in HALO™.**

(A) Raw nasal turbinate with nuclei shown in blue (I.e., hematoxylin counter stain) and spike immunoreactivity in brown.

(B) Correlating positive pixel analysis output of HCoV-OC43 spike area quantification (AQ) with nuclei shown in blue and spike immunoreactivity in yellow.

## RESULTS

### Depletion of type-I IFN signaling does not increase disease susceptibility to HCoV-OC43 infection in mice

C57BL/6 and IFNAR  $-/-$  mice of both sexes were inoculated intranasally with HCoV-OC43 with endpoints two- and seven-days post-infection. Both strains of mice were inoculated with either  $10^4$  (low) or  $10^6$  (high) FFU dose and show no clear differences in clinical score, weight changes, or temperature changes as seen in **Figure 5. Table 7** highlights the specific criteria utilized for clinical scoring.

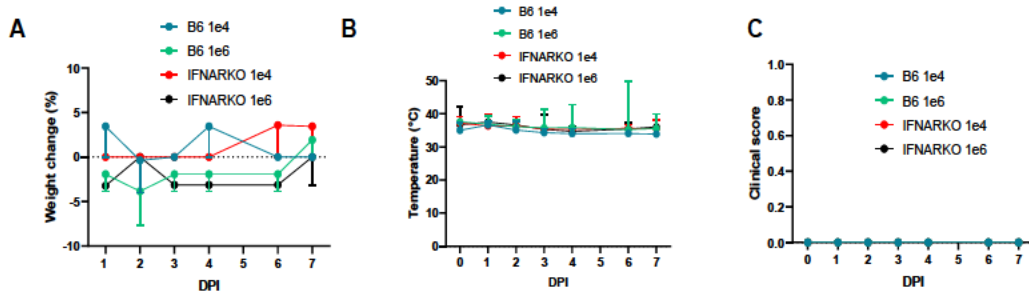


**Figure 5. HCoV-OC43 caused no lethal disease in INFAR-KO  $-/-$  and C57BL/6 wild type mice.**

IFNAR-KO  $-/-$  mice (n=24, (male n=12; 104 n=6, 106 n=6), (female n=12; 104 n=6, 106 n=6),) and C57BL/6 mice (n=24 (male n=12; 104 n=6, 106 n=6), (female n=12; 104 n=6, 106 n=6)) were inoculated with either a low dose or high dose of HCoV-OC43 intranasally ( $10^4$  or  $10^6$  focus forming units (FFU)). Body weight (A), Temperature (B) and Clinical score (C) were recorded daily. Mice were injected intraperitoneally with a UID chip prior infection in order to measure body temperatures daily.

**IFNAR <sup>-/-</sup> mice display increased pathology in nasal passages upon HCoV-OC43 infection**

Histopathology of the nasal passages were examined in C57BL/6 and IFNAR <sup>-/-</sup> mice following HCoV-OC43 infection. Minimal findings irrespective of mice genotype and viral dose were observed with the exception of rare, localized rhinitis and edema at the level of the squamous epithelium at seven days post-infection. IFNAR <sup>-/-</sup> mice inoculated with high doses displayed a higher frequency of histopathology (five out of the twelve mice) compared to the C57BL/6 at day 7 post-infection as seen in **Table 9**. Only two of the C57BL/6 inoculated with the low virus dose displayed histopathology while none of the mice inoculated with the high dose displayed histopathology (**Figure 6**).

Mice Strain:	C57BL/6 (n = 12)		IFNAR <sup>-/-</sup> (n = 12)	
	2 DPI	7 DPI	2 DPI	7 DPI
<b>Endpoints in DPI (Days post-infection)</b>				
<b>No histopathology observed in nasal passages</b>	6	6	6	1
<b>Histopathology observed in nasal passages</b>	0	0	0	5

**Table 9.** frequencies of mice challenged with a high dose of 1.00E +6 FFU of HCoV-OC43 displaying histopathology.

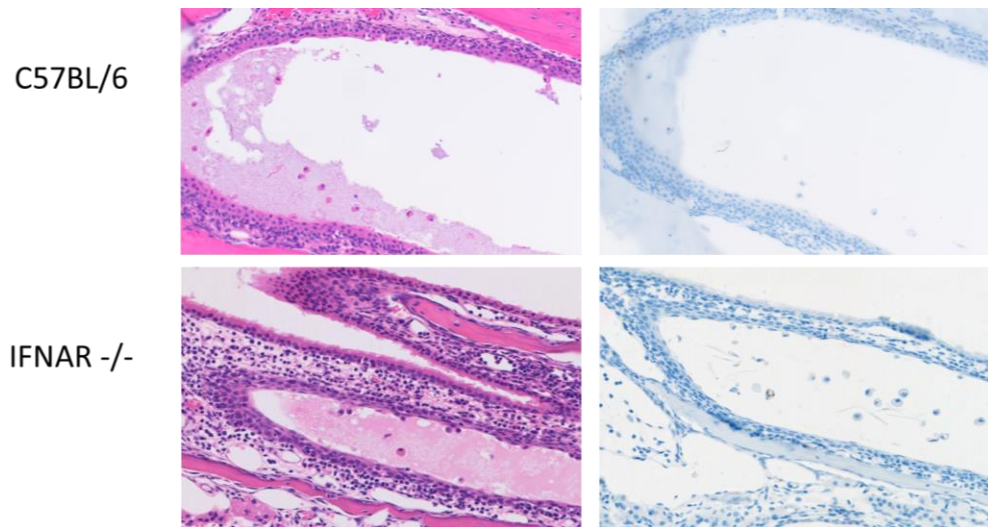


**Figure 6. H&E and anti-Spike staining in the nasal passages of IFNAR -/- and C57BL/6 mice following HCoV-OC43 infection at day 7 post-infection.**

C57BL/6 mice and IFNAR -/- mice were inoculated with  $10^6$  FFU of HCoV-OC43. H&E staining (Left panels) and anti-Spike immunohistochemistry (Right panels) in the nasal passages were performed. No significant histopathological differences were seen between the two models at that viral dose with exceptions of mild edema at 7 days post-infection.

Sex	STRAIN	VIRUS	DOSE	DPI	Histologic findings	Morphologic diagnosis	Spike IHC
M	C57BL/6	HCoV-OC43	1.00E+04 PFU	7	Mild focal neutrophilic infiltrate of respiratory epithelium with segmental squamous metaplasia	Rhinitis, neutrophilic, mild, segmental, with squamous metaplasia	0
M	C57BL/6	HCoV-OC43	1.00E+06 PFU	2	NSF		0
M	C57BL/6	HCoV-OC43	1.00E+06 PFU	2	NSF		0
F	C57BL/6	HCoV-OC43	1.00E+06 PFU	2	NSF		0
F	C57BL/6	HCoV-OC43	1.00E+06 PFU	2	NSF		0
M	C57BL/6	HCoV-OC43	1.00E+06 PFU	7	NSF		0
F	C57BL/6	HCoV-OC43	1.00E+04 PFU	7	Minimal submucosal neutrophilic infiltrate at the level of squamous epithelium with rare denuded squamous epithelium and minimal edema in adjacent meatus.	Rhinitis, neutrophilic, mild, with denuded squamous epithelium and edema	0
M	C57BL/6	HCoV-OC43	1.00E+04 PFU	7	NSF		0
M	C57BL/6	HCoV-OC43	1.00E+04 PFU	7	NSF		0
M	C57BL/6	HCoV-OC43	1.00E+04 PFU	7	NSF		0
M	C57BL/6	HCoV-OC43	1.00E+06 PFU	7	NSF		0
M	C57BL/6	HCoV-OC43	1.00E+04 PFU	2	NSF		0
M	C57BL/6	HCoV-OC43	1.00E+04 PFU	2	NSF		0
F	C57BL/6	HCoV-OC43	1.00E+06 PFU	7	NSF		0
F	C57BL/6	HCoV-OC43	1.00E+06 PFU	7	NSF		0
F	C57BL/6	HCoV-OC43	1.00E+06 PFU	7	NSF		0
F	C57BL/6	HCoV-OC43	1.00E+04 PFU	2	NSF		0
F	C57BL/6	HCoV-OC43	1.00E+04 PFU	2	NSF		0
F	C57BL/6	HCoV-OC43	1.00E+04 PFU	2	NSF		0
M	C57BL/6	HCoV-OC43	1.00E+06 PFU	2	NSF		1 (Olfactory epithelium)
F	C57BL/6	HCoV-OC43	1.00E+06 PFU	2	NSF		2 (Olfactory epithelium)
F	IFNAR -/-	HCoV-OC43	1.00E+06 PFU	7	Mild neutrophilic and lymphocytic infiltrate of the submucosa at the level of the squamous epithelium with localized denuding of squamous epithelium into adjacent meatus with edema.	Rhinitis, neutrophilic and lymphocytic, mild, with denuded squamous epithelium and edema	0
M	IFNAR -/-	HCoV-OC43	1.00E+06 PFU	7	Mild neutrophilic and lymphocytic infiltrate of the submucosa at the level of the squamous epithelium with localized denuding of squamous epithelium into adjacent meatus with intralesional edema.	Rhinitis, neutrophilic and lymphocytic, mild, with denuded squamous epithelium and edema	0
F	C57BL/6	HCoV-OC43	1.00E+04 PFU	7	NSF		0
F	C57BL/6	HCoV-OC43	1.00E+04 PFU	7	NSF		0
M	IFNAR -/-	HCoV-OC43	1.00E+06 PFU	7	Mild neutrophilic and lymphocytic infiltrate of the submucosa at the level of the squamous epithelium with localized denuding of squamous epithelium into adjacent meatus with intralesional edema.	Rhinitis, neutrophilic and lymphocytic, mild, with denuded squamous epithelium and edema	0
M	IFNAR -/-	HCoV-OC43	1.00E+04 PFU	7	NSF		0
M	IFNAR -/-	HCoV-OC43	1.00E+04 PFU	7	NSF		0
M	IFNAR -/-	HCoV-OC43	1.00E+04 PFU	7	NSF		0
M	IFNAR -/-	HCoV-OC43	1.00E+04 PFU	2	NSF		0
M	IFNAR -/-	HCoV-OC43	1.00E+04 PFU	2	NSF		0
F	IFNAR -/-	HCoV-OC43	1.00E+04 PFU	2	NSF		0
F	IFNAR -/-	HCoV-OC43	1.00E+04 PFU	2	NSF		0
F	IFNAR -/-	HCoV-OC43	1.00E+04 PFU	2	NSF		0
F	IFNAR -/-	HCoV-OC43	1.00E+04 PFU	7	NSF		0
F	IFNAR -/-	HCoV-OC43	1.00E+04 PFU	7	NSF		0
F	IFNAR -/-	HCoV-OC43	1.00E+04 PFU	7	NSF		0
F	IFNAR -/-	HCoV-OC43	1.00E+04 PFU	7	NSF		0
F	IFNAR -/-	HCoV-OC43	1.00E+04 PFU	7	NSF		0
F	IFNAR -/-	HCoV-OC43	1.00E+06 PFU	7	Mild neutrophilic and lymphocytic infiltrate of the submucosa at the level of the squamous epithelium with localized denuding of squamous epithelium into adjacent meatus with intralesional bacteria and edema.	Rhinitis, neutrophilic and lymphocytic, mild, with denuded squamous epithelium, edema, and intralesional bacteria	0
M	IFNAR -/-	HCoV-OC43	1.00E+06 PFU	7	Mild to moderate neutrophilic and lymphocytic infiltrate of the submucosa at the level of the squamous and respiratory epithelium with localized denuding of squamous epithelium into adjacent meatus with intralesional edema. Focal luminal proteinaceous fluid accumulation in ethmoidal turbinate meatus with low numbers of intralesional neutrophils and denuded olfactory epithelium. Adjacent ON is multifocally vacuolated and disorganized (presumed degeneration).	Rhinitis, neutrophilic and lymphocytic, mild, with denuded squamous epithelium and edema; Olfactory epithelial degeneration (presumptive), mild, localized, with mild luminal neutrophilic exudate, and denuded OE	0
M	IFNAR -/-	HCoV-OC43	1.00E+06 PFU	2	NSF		0
F	IFNAR -/-	HCoV-OC43	1.00E+06 PFU	7	NSF		0
M	IFNAR -/-	HCoV-OC43	1.00E+06 PFU	2	NSF		1 (Olfactory epithelium)
F	IFNAR -/-	HCoV-OC43	1.00E+06 PFU	2	NSF		1 (Olfactory epithelium)
F	IFNAR -/-	HCoV-OC43	1.00E+06 PFU	2	NSF		2 (Olfactory epithelium)
F	IFNAR -/-	HCoV-OC43	1.00E+06 PFU	2	NSF		2 (Olfactory epithelium)
M	IFNAR -/-	HCoV-OC43	1.00E+06 PFU	2	NSF		2 (Olfactory epithelium)

**Table 10. Histopathology summary of the nasal passages of IFNAR-/- and C57BL/6 mice infected with different doses of HCoV-OC43.**

In addition to the low and high infectious doses, we also inoculated mice with a viral dose of  $10^7$  FFU. Interestingly, minimal histopathological manifestations of infection were observed only in IFNAR  $-/-$  mice at day 5 post-infection (**Table 11**). These manifestations were characterized by localized rhinitis, edema, and mild inflammation at the level of the respiratory epithelium (**Tables 12 and 13**). **Figure 7** highlights the detectable immunoreactive cells for the spike antigen in the nasal passages. However, no spike immunoreactivity was observed in the respiratory epithelium.

Mice strain	C57BL/6 (n=12)				IFNAR $-/-$ (n = 34)			
	1 DPI	3 DPI	5 DPI	7 DPI	1 DPI	3 DPI	5 DPI	7 DPI
Endpoints in DPI (Days post-infection)								
No histopathology observed in nasal passages	<b>4</b>	<b>4</b>	<b>4</b>	<b>4</b>	<b>4</b>	<b>10</b>	<b>4</b>	<b>7</b>
Histopathology observed in nasal passages	<b>0</b>	<b>0</b>	<b>0</b>	<b>0</b>	<b>0</b>	<b>1</b>	<b>6</b>	<b>0</b>

**Table 11. frequencies of mice challenged with a high dose  $1.00E+7$  FFU of HCoV-OC43 displaying histopathology in the nasal passages.**

IFNAR  $-/-$  mice have a higher frequency of displaying histologic hallmarks at a higher dose than the C57BL/6 wild type. Control mice inoculated with sham/PBS and C57BL/6 wild-type mice from 2 days post-infection display no histological hallmarks and were excluded from this table as no IFNAR  $-/-$  has an endpoint of 2 dpi.

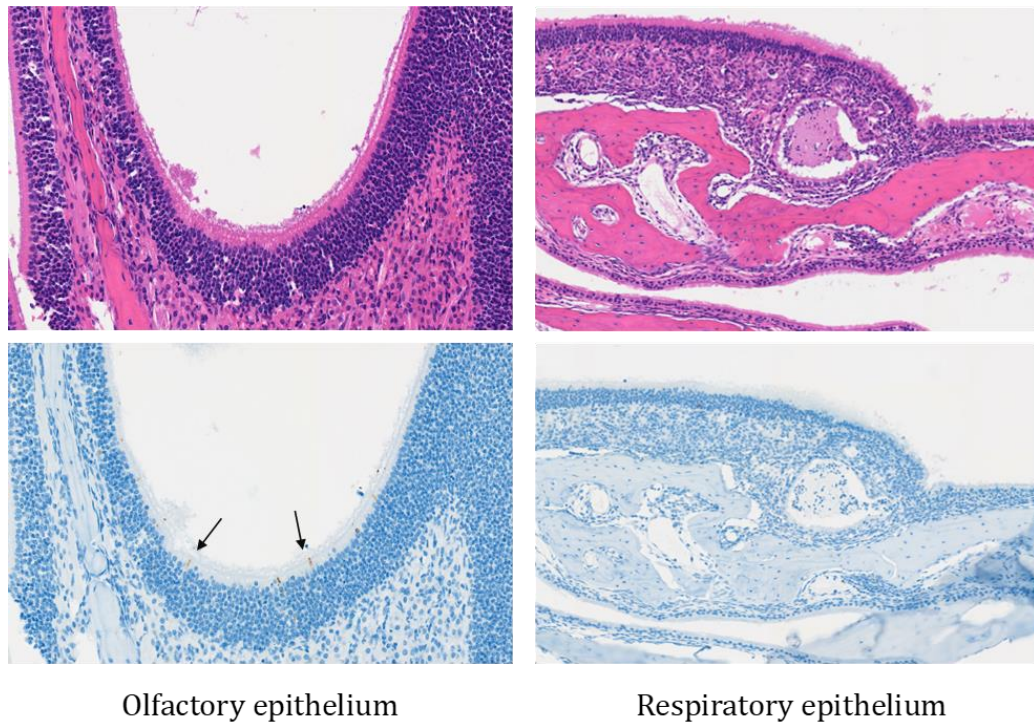


**Figure 7. H&E and anti-Spike staining in the nasal passages of IFNAR  $-/-$  mice following HCoV-OC43 infection ( $10^7$  FFU) at day 5 post-infection.**

IFNAR  $-/-$  mice were inoculated with  $10^7$  FFU of HCoV-OC43. H&E staining (Top panels) and anti-Spike immunohistochemistry (Bottom panels) in the olfactory (left panels) and respiratory (right panels) epithelium were performed. Black arrows indicate spike-positive cells.

ANIMALID	Sex	STRAIN	VIRUS	DOSE	DPI	Nasal passage histologic findings	Morphologic diagnosis	Spike IHC	Lung histologic findings	Spike IHC
1-3DPI	M	IFNAR -/-	HCoV-OC43	IFNAR -/- 1E7 (3 DPI)	3 DPI	NSF		2 (Olfactory epithelium)	NE	NE
2-3DPI	F	IFNAR -/-	HCoV-OC43	IFNAR -/- 1E7 (3 DPI)	3 DPI	NSF		2 (Olfactory epithelium)	NSF	0
3-3DPI	F	IFNAR -/-	HCoV-OC43	IFNAR -/- 1E7 (3 DPI)	3 DPI	NSF		2 (Olfactory epithelium)	Scant focal interstitial mononuclear infiltrate	0
4-3DPI	M	IFNAR -/-	HCoV-OC43	IFNAR -/- 1E7 (3 DPI)	3 DPI	NSF		2 (Olfactory epithelium)	Scant perivascular mononuclear infiltrate	1 (scant rare single pneumocyte)
5-3DPI	M	IFNAR -/-	HCoV-OC43	IFNAR -/- 1E7 (3 DPI)	3 DPI	NSF		2 (Olfactory epithelium)	NE	NE
6-3DPI	F	IFNAR -/-	HCoV-OC43	IFNAR -/- 1E7 (3 DPI)	3 DPI	NSF		2 (Olfactory epithelium)	NE	NE
7-3DPI	F	IFNAR -/-	HCoV-OC43	IFNAR -/- 1E7 (3 DPI)	3 DPI	NSF		2 (Olfactory epithelium)	NE	NE
1-5DPI	F	IFNAR -/-	HCoV-OC43	IFNAR -/- 1E7 (5 DPI)	5 DPI	Mild neutrophilic and mononuclear infiltrate in respiratory epithelium submucosa	Rhinitis, neutrophilic and mononuclear, mild	2 (Olfactory epithelium)	NSF	0
2-5DPI	F	IFNAR -/-	HCoV-OC43	IFNAR -/- 1E7 (5 DPI)	5 DPI	Mild neutrophilic and mononuclear infiltrate in respiratory epithelium submucosa	Rhinitis, neutrophilic and mononuclear, mild	1 (Olfactory epithelium)	NSF	0
3-5DPI	M	IFNAR -/-	HCoV-OC43	IFNAR -/- 1E7 (5 DPI)	5 DPI	Moderate neutrophilic and mononuclear infiltrate, edema, and ectasia of submucosal glands in respiratory epithelium	Rhinitis, neutrophilic and mononuclear, moderate with edema, and ductular degeneration	1 (Olfactory epithelium)	NSF	0
4-5DPI	M	IFNAR -/-	HCoV-OC43	IFNAR -/- 1E7 (5 DPI)	5 DPI	Mild neutrophilic and mononuclear infiltrate in respiratory epithelium submucosa	Rhinitis, neutrophilic and mononuclear, mild	2 (Olfactory epithelium)	NE	NE
5-5DPI	M	IFNAR -/-	HCoV-OC43	IFNAR -/- 1E7 (5 DPI)	5 DPI	Moderate neutrophilic and mononuclear infiltrate, edema, and ectasia of submucosal glands in respiratory epithelium	Rhinitis, neutrophilic and mononuclear, moderate with edema, and ductular degeneration	1 (Olfactory epithelium)	NE	NE
6-5DPI	F	IFNAR -/-	HCoV-OC43	IFNAR -/- 1E7 (5 DPI)	5 DPI	NSF		1 (Olfactory epithelium)	NE	NE
1-7DPI	M	IFNAR -/-	HCoV-OC43	IFNAR -/- 1E7 (5 DPI)	7 DPI	NSF		0	Mild perivascular and peribronchiolar mononuclear infiltrate	0
2-7DPI	M	IFNAR -/-	HCoV-OC43	IFNAR -/- 1E7 (5 DPI)	7 DPI	NSF		0	NE	NE
3-7DPI	F	IFNAR -/-	HCoV-OC43	IFNAR -/- 1E7 (5 DPI)	7 DPI	NSF		0	Scant perivascular and peribronchiolar mononuclear infiltrate	0
4-7DPI	M	IFNAR -/-	HCoV-OC43	IFNAR -/- 1E7 (5 DPI)	7 DPI	NSF		0	Scant perivascular mononuclear infiltrate	0
5-7DPI	F	IFNAR -/-	HCoV-OC43	IFNAR -/- 1E7 (5 DPI)	7 DPI	NSF		0	NE	NE
6-7DPI	F	IFNAR -/-	HCoV-OC43	IFNAR -/- 1E7 (5 DPI)	7 DPI	NSF		0	NE	NE
7-7DPI	M	IFNAR -/-	HCoV-OC43	IFNAR -/- 1E7 (5 DPI)	7 DPI	NSF		0	NE	NE
Sham/MOCK	F	IFNAR -/-	Mock	non-infected	5 DPI	NSF		0	NE	NE

**Table 12. Histopathology summary of the nasal passages of IFNAR<sup>-/-</sup> and C57BL/6 mice infected with 107 FFU of HCoV-OC43.**

NIMAL	Sex	STRAIN	VIRUS	DOSE	DPI	Nasal passage histologic findings	Morphologic diagnosis	Spike IHC	Lung histologic findings	Spike IHC
1-3DPI	M	IFNAR -/-	HCoV-OC43	IFNAR -/- 1E7 (3 DPI)	3 DPI	NSF		2 (Olfactory epithelium)	NE	NE
2-3DPI	F	IFNAR -/-	HCoV-OC43	IFNAR -/- 1E7 (3 DPI)	3 DPI	NSF		2 (Olfactory epithelium)	NSF	0
3-3DPI	F	IFNAR -/-	HCoV-OC43	IFNAR -/- 1E7 (3 DPI)	3 DPI	NSF		2 (Olfactory epithelium)	Scant focal interstitial mononuclear infiltrate	0
4-3DPI	M	IFNAR -/-	HCoV-OC43	IFNAR -/- 1E7 (3 DPI)	3 DPI	NSF		2 (Olfactory epithelium)	Scant perivascular mononuclear infiltrate	1 (scant rare single pneumocyte)
5-3DPI	M	IFNAR -/-	HCoV-OC43	IFNAR -/- 1E7 (3 DPI)	3 DPI	NSF		2 (Olfactory epithelium)	NE	NE
6-3DPI	F	IFNAR -/-	HCoV-OC43	IFNAR -/- 1E7 (3 DPI)	3 DPI	NSF		2 (Olfactory epithelium)	NE	NE
7-3DPI	F	IFNAR -/-	HCoV-OC43	IFNAR -/- 1E7 (3 DPI)	3 DPI	NSF		2 (Olfactory epithelium)	NE	NE
1-5DPI	F	IFNAR -/-	HCoV-OC43	IFNAR -/- 1E7 (5 DPI)	5 DPI	Mild neutrophilic and mononuclear infiltrate in respiratory epithelium submucosa	Rhinitis, neutrophilic and mononuclear, mild	2 (Olfactory epithelium)	NSF	0
2-5DPI	F	IFNAR -/-	HCoV-OC43	IFNAR -/- 1E7 (5 DPI)	5 DPI	Mild neutrophilic and mononuclear infiltrate in respiratory epithelium submucosa	Rhinitis, neutrophilic and mononuclear, mild	1 (Olfactory epithelium)	NSF	0
3-5DPI	M	IFNAR -/-	HCoV-OC43	IFNAR -/- 1E7 (5 DPI)	5 DPI	Moderate neutrophilic and mononuclear infiltrate, edema, and ectasia of submucosal glands in respiratory epithelium	Rhinitis, neutrophilic and mononuclear, moderate with edema, and ductular degeneration	1 (Olfactory epithelium)	NSF	0
4-5DPI	M	IFNAR -/-	HCoV-OC43	IFNAR -/- 1E7 (5 DPI)	5 DPI	Mild neutrophilic and mononuclear infiltrate in respiratory epithelium submucosa	Rhinitis, neutrophilic and mononuclear, mild	2 (Olfactory epithelium)	NE	NE
5-5DPI	M	IFNAR -/-	HCoV-OC43	IFNAR -/- 1E7 (5 DPI)	5 DPI	Moderate neutrophilic and mononuclear infiltrate, edema, and ectasia of submucosal glands in respiratory epithelium	Rhinitis, neutrophilic and mononuclear, moderate with edema, and ductular degeneration	1 (Olfactory epithelium)	NE	NE
6-5DPI	F	IFNAR -/-	HCoV-OC43	IFNAR -/- 1E7 (5 DPI)	5 DPI	NSF		1 (Olfactory epithelium)	NE	NE
1-7DPI	M	IFNAR -/-	HCoV-OC43	IFNAR -/- 1E7 (5 DPI)	7 DPI	NSF		0	Mild perivascular and peribronchiolar mononuclear infiltrate	0
2-7DPI	M	IFNAR -/-	HCoV-OC43	IFNAR -/- 1E7 (5 DPI)	7 DPI	NSF		0	NE	NE
3-7DPI	F	IFNAR -/-	HCoV-OC43	IFNAR -/- 1E7 (5 DPI)	7 DPI	NSF		0	Scant perivascular and peribronchiolar mononuclear infiltrate	0
4-7DPI	M	IFNAR -/-	HCoV-OC43	IFNAR -/- 1E7 (5 DPI)	7 DPI	NSF		0	Scant perivascular mononuclear infiltrate	0
5-7DPI	F	IFNAR -/-	HCoV-OC43	IFNAR -/- 1E7 (5 DPI)	7 DPI	NSF		0	NE	NE
6-7DPI	F	IFNAR -/-	HCoV-OC43	IFNAR -/- 1E7 (5 DPI)	7 DPI	NSF		0	NE	NE
7-7DPI	M	IFNAR -/-	HCoV-OC43	IFNAR -/- 1E7 (5 DPI)	7 DPI	NSF		0	NE	NE
am/MO	F	IFNAR -/-	Mock	non-infected	5 DPI	NSF		0	NE	NE

**Table 13. Histopathology summary of the nasal passages of IFNAR-/- mice infected with 107 FFU of HCoV-OC43 (second cohort).**

### Increased HCoV-OC43 replication in the nasal passages of IFNAR $-/-$ mice

Nasal passages stained with our polyclonal anti-Spike antibody displayed immunoreactive cells exclusively in the olfactory epithelium. Ordinal scoring of immunoreactivity revealed that with the low viral dose, no mice (either mouse strain) displayed spike antigen. However, when IFNAR  $-/-$  and C57BL/6 were inoculated with  $10^6$  FFU, they displayed immunoreactive cells. Ordinal scoring for IFNAR  $-/-$  mice inoculated with this viral dose showed elevated levels of spike antigen at 2 days post-infection while very few C57BL/6 displayed immunoreactive cells (**Figure 8**). By seven days post-infection irrespective of dose and genotype, no mice scored for immunoreactivity. Representative images in **Figure 9** display representative immunohistochemistry pictures with detectable antigen in the olfactory epithelium.

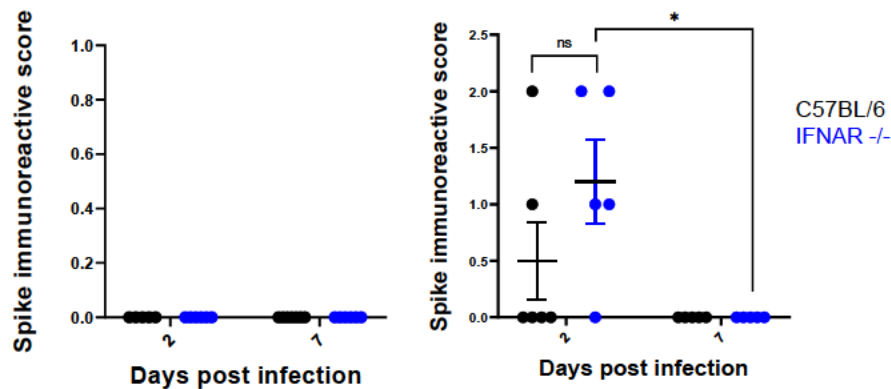


**Figure 8. Ordinal scoring of immunohistochemistry targeting HCoV-OC43 spike in the nasal passages of infected C57BL/6 and IFNAR  $-/-$  mice.**

(A) IFNAR  $-/-$  and C57BL/6 wild-type inoculated with  $10^4$  FFU did not contain any positive cells for the HCoV-OC43 spike.

(B) IFNAR  $-/-$  and C57BL/6 wild type inoculated with  $10^6$  FFU show elevated levels of spike immunoreactivity at two days post-infection.

Scoring was as follows; 0 = no immunoreactivity observed, 1 = rare single cell immunoreactivity, 2 = multifocal small sporadic aggregates of immunoreactive cells. Statistical significance was determined using Mann-Withney unpaired T-test. Significant levels; \* $<0.05$ , \*\* $<0.01$

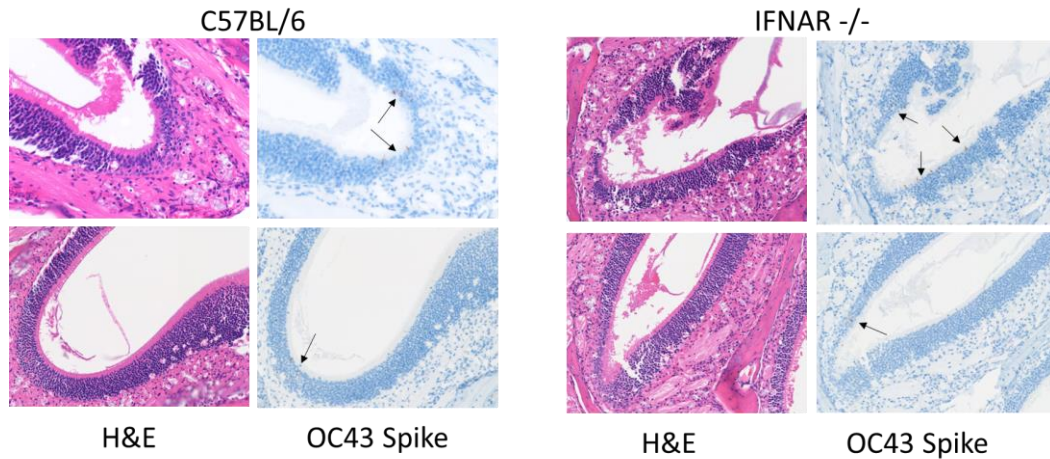


**Figure 9. HCoV-OC43 spike antigen is detectable within the olfactory epithelium**

Spike antigen present in the absence of overt cytopathic effect at 2 days post-infection in IFNAR  $-/-$  mice intranasally inoculated with  $10^6$  FFU of HCoV-OC43.

C57BL/6 and IFNAR  $-/-$  mice were inoculated with  $10^7$  FFU of HCoV-OC43. H&E staining (Left panels) and anti-Spike immunohistochemistry (Right panels) was performed on day 2 post-infection. Black arrows indicate spike-positive cells.

Quantification of Spike immunoreactive cells supported evidence that IFNAR  $-/-$  mice have elevated levels of spike antigen in the olfactory epithelium at two days post-infection compared to the C57BL/6 mice. Additionally, at seven days post-infection, both genotypes contained little to no immunoreactive cells. **Figure 10** highlights these trends with representative images



Upon infection with  $10^7$  FFU, ordinal scoring of the spike immunoreactivity in IFNAR  $-/-$  mice resulted in even higher scores in the olfactory epithelium compared to C57BL/6 mice **Figure 11**). Quantification of Spike immunoreactivity resulted in statistical significance between IFNAR  $-/-$  and C57BL/6 mice at all time points as seen in **Figure 12**. It is noteworthy that our findings indicate that the day three post-infection timepoint constitutes the peak of viral antigen. By five days post-infection, both genotypes resulted in a decrease in spike immunoreactivity.

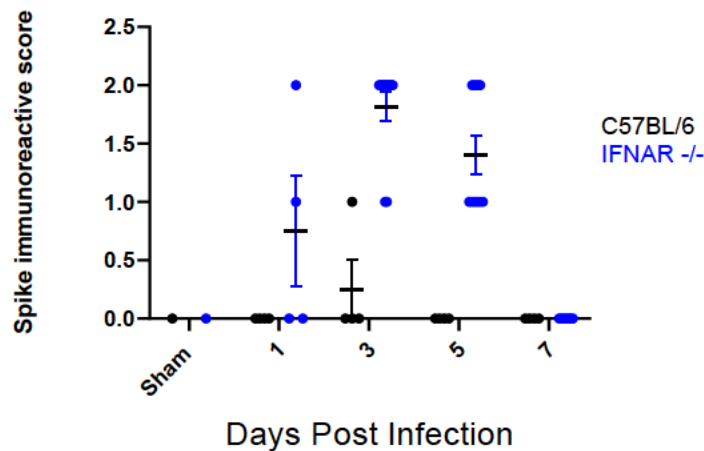


**Figure 11. Ordinal spike immunoreactivity score in C57BL/6 wild type vs. IFNAR  $-/-$  mice**

At 1DPI, 3DPI, 5DPI, and 7DPI IFNAR  $-/-$  mice exhibit more spike immunoreactivity compared to wild type (IFNAR  $-/-$  n= 33 (male, n =17; female, n =16 ), C57BL/6 n= 21 (male n= 9; female n = 12)) inoculated with  $1.00E+7$  FFU of HCoV-OC43.

Scoring was as follows; 0 = no immunoreactivity observed, 1 = rare single cell immunoreactivity, 2 = multifocal small sporadic aggregates of immunoreactive cells. Statistical significance was determined using Mann-Whitney unpaired T-test. Significant levels; \* $<0.05$ , \*\* $<0.01$ , \*\*\*  $p \leq 0.001$  \*\*\*\*  $p \leq 0.000$

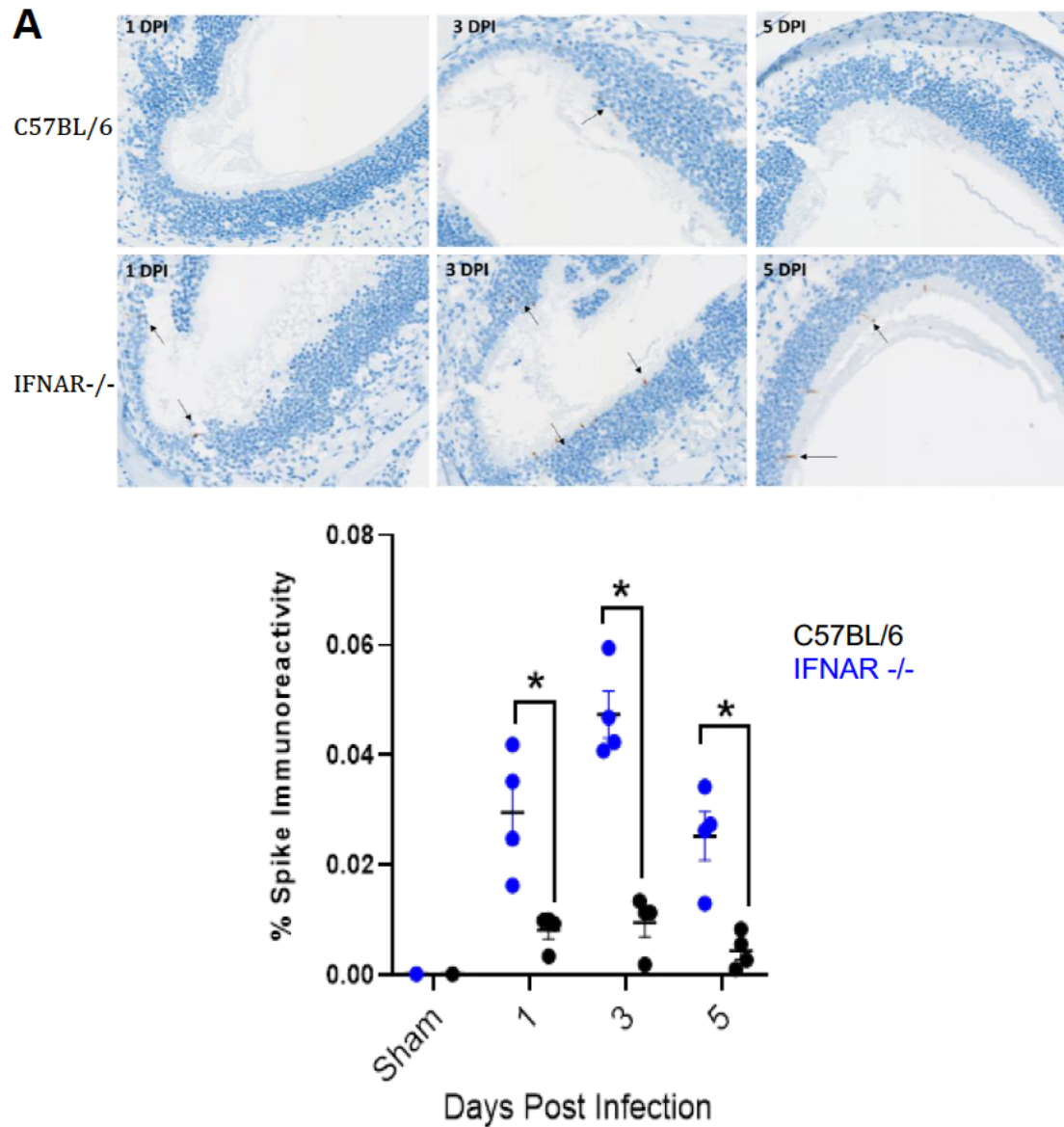


**Figure 12. IFNAR<sup>-/-</sup> mice show a peak of Spike antigens at day 3 post-infection compared to C57BL/6 mice.**

- (A) Representative pictures of anti-Spike immunohistochemistry of the nasal passages of C57BL/6 and IFNAR<sup>-/-</sup> mice at day 1, 3, and 5 post-infection following infection with  $10^7$  FFU of HCoV-OC43.
- (B) Quantification of Spike immunoreactivity for each mouse model and time points following infection with  $10^7$  FFU of HCoV-OC43. Statistical significance was determined using Mann-Whitney unpaired T-test. Significant levels; \* $<0.05$ , \*\* $<0.01$

Interestingly, anti-Spike immunohistochemistry using an anti-Spike monoclonal antibody (developed as a follow-up of our polyclonal antibody by our industry partner) provided a stronger appreciation of the increased susceptibility of IFNAR  $-/-$  mice to HCoV-OC43 infection (**Figure 13**). Quantification of spike immunoreactivity using this novel antibody on tissue sections from IFNAR  $-/-$  nasal passages ( $10^7$  FFU infectious dose) resulted in a near 10-fold signal increase when compared to the polyclonal chromogenic staining. Immunoreactivity quantification following staining with this novel antibody provided overall a more robust validation of the increased susceptibility of IFNAR  $-/-$  mice to HCoV-OC43 infection. Our results also confirmed the viral replication kinetics previously observed with the polyclonal antibody in the nasal passages of IFNAR  $-/-$  mice infected with  $10^7$  FFU, characterized by a peak of viral replication at day 3 post-infection prior to viral clearance at day 7 post-infection.

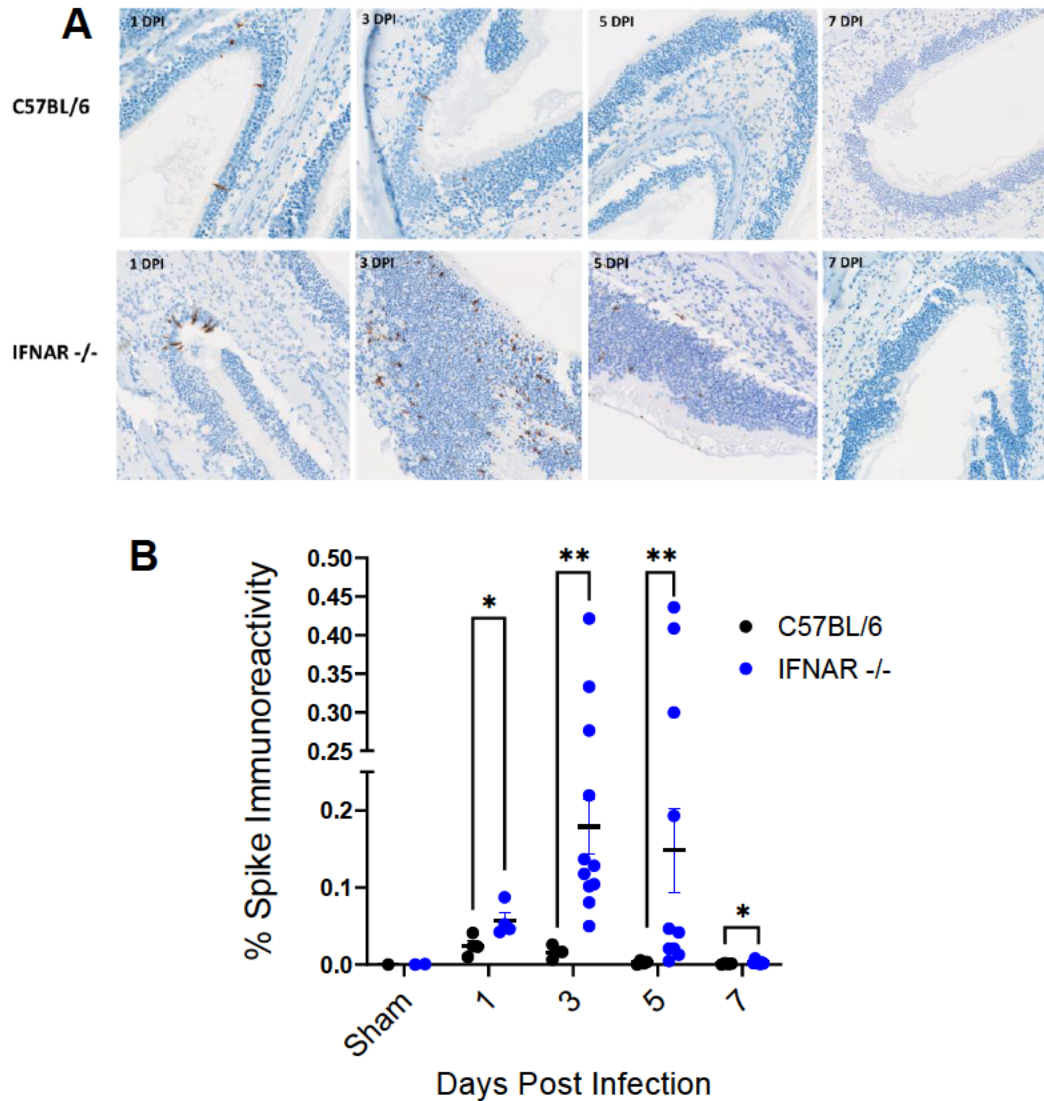


**Figure 13. A monoclonal anti-Spike antibody confirm increased susceptibility of IFNAR<sup>-/-</sup> mice to HCoV-OC43 infection.**

(A) Representative pictures of anti-Spike immunohistochemistry (using a novel monoclonal antibody) of the nasal passages of C57BL/6 and IFNAR<sup>-/-</sup> mice at day 1, 3, 5, and 7 post-infection following infection with  $10^7$  FFU of HCoV-OC43.

(B) Quantification of Spike immunoreactivity for each mouse model and time points following infection with  $10^7$  FFU of HCoV-OC43. Statistical significance was determined using Mann-Whitney unpaired T-test. Significant levels; \* $<0.05$ , \*\* $<0.01$

### HCoV-OC43 does not effectively replicate in the lung of IFNAR $-/-$ mice

In the lower respiratory tract (lung), as seen in **figure 14**, C57BL/6 and IFNAR  $-/-$  inoculated with  $10^6$  FFU displayed no clear differences in viral RNA copy number at both two-and-seven days post-infection. Similar conclusions were also made upon infection with  $10^7$  FFU (**Figure 14**). However, it was worth noting that at this infectious dose, while lung viral load in C57BL/6 incrementally decreased, the viral load in infected IFNAR  $-/-$  persisted, indirectly suggesting a potential superior albeit limited ability of this mouse model to support viral replication in the lung. However, we were not able to detect any infectious particles from the lung of infected IFNAR  $-/-$  mice at any time points (data not shown), confirming limited to no lung viral replication. It is also likely that such assay may not provide the sensitivity required to detect a limited amount of infectious viral particles in tissues.

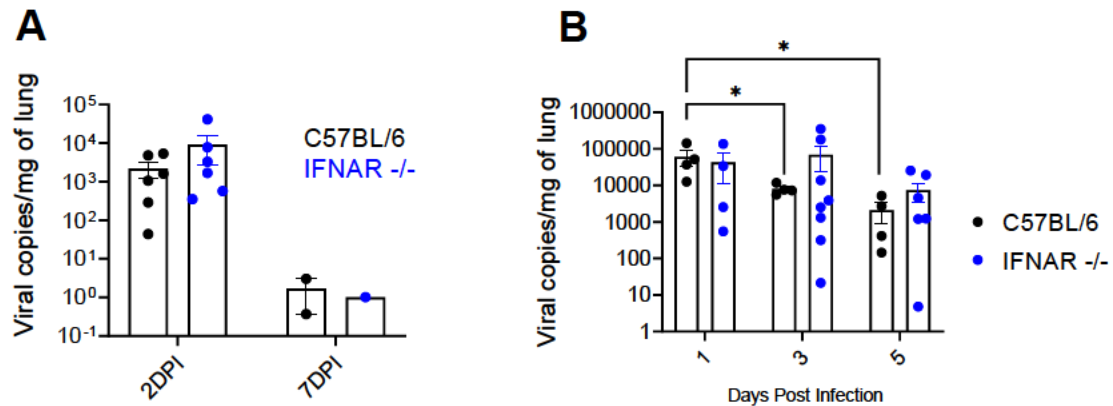


**Figure 14. comparison of viral RNA copies and qPCR**

(A) C57BL/6 and IFNAR  $-/-$  inoculated with  $1.00E+6$  FFU of HCoV-OC43

(B) C57BL/6 wild type and IFNAR  $-/-$  mice inoculated with  $1.00E+7$  FFU of HCoV-OC43.

RT-qPCR of homogenized mice lungs show no clear differences, and by day seven post-infection, RNA/mg of tissue was undetectable. Statistical significance was determined using the Mann-Whitney unpaired T-test. Significant levels; \* $<0.05$ , \*\* $<0.01$

In addition, whole lungs were inflated using a low melting point of 1 x agarose in sterile PBS (phosphate-buffered saline). Slides were stained for hematoxylin and eosin (H&E) in order to observe key histopathologic characteristics and immunohistochemistry for the HCoV-OC43 spike protein was performed. Lung histopathology analysis showed that very few IFNAR  $-/-$  mice displayed scant or mild perivascular and peribronchiolar monocular infiltrates. at 7 days post-infection. (images not shown) Additionally, only one IFNAR  $-/-$  mouse displayed rare scant immunoreactivity for spike in the lungs (representative images not shown). Altogether this data is consistent with our viral load quantification findings and suggest that viral replication in IFNAR  $-/-$  is restricted to the nasal passages and does not spread to the respiratory tract.

### Approaching the role of type-III IFN in preventing HCoV-OC43 dissemination in the lower respiratory tract

Considering previous evidence that type III IFN signaling restricts the dissemination of respiratory viruses to the respiratory tract, we then wanted to determine whether such a signaling pathway restricts HCoV-OC43 infection in IFNAR  $-/-$  mice. IFNAR  $-/-$  mice of both sexes were intranasally treated with a control isotype antibody (IgG) or an anti-IFN $\lambda$ 2 one day prior to infection and eight hours post-infection. Another group of mice was not treated at all. At the 3 days post-infection, mice were euthanized, and tissues (nasal passages and lungs) were collected. At that time point, none of the experimental groups showed a significant difference in percent weight loss from the initial weight taken on the day of infection. (**figure 15**).

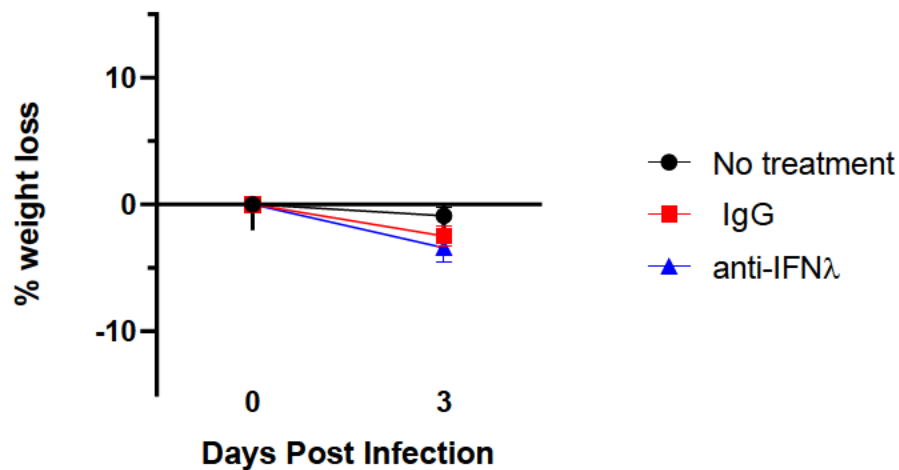


**Figure 15.** Percent of weight loss between IFNAR  $-/-$  treated with anti-IFN $\lambda$ 2, IgG or non-treated upon infection with HCoV-OC43 ( $10^7$  FFU).

Interestingly, albeit histopathological manifestations of disease were overall between the different experimental conditions IFNAR<sup>-/-</sup> mice, IFNAR<sup>-/-</sup> treated with anti-IFN $\lambda$ 2 showed more peracute inflammation in the nasal passages. Furthermore, immunohistochemistry staining showed that anti-IFN $\lambda$ 2 treatment led to Spike immunoreactivity extending into the respiratory epithelium. Qualitatively, anti-IFN  $\lambda$ 2 treatment also appears to result in a more abundant viral antigen that extends more proximally in the nasal passages and is observed with the submucosal inflammatory infiltrates (and rarely with the respiratory epithelium) as seen in **Figure 16**. No viral antigens were however detected in the lower respiratory tract. Altogether, these findings represent preliminary evidence that type III IFN signaling contributes to restricting HCoV-OC43 dissemination into the respiratory tract.

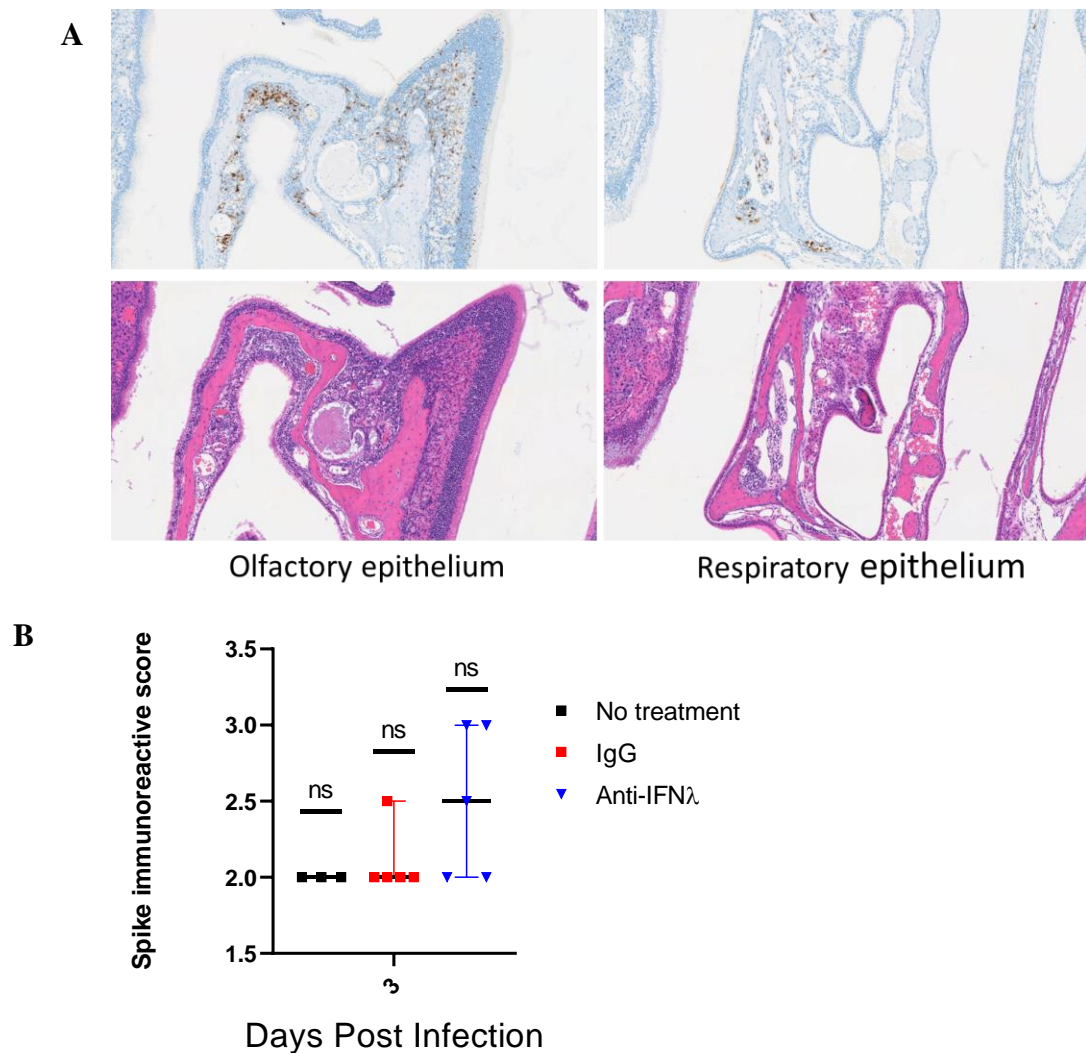


**Figure 16. IFNAR  $-/-$  mice treated with anti-IFN $\lambda$ 2 are more permissive to HCoV-OC43 replication in the nasal passages**

(A) Ordinal scoring of immunohistochemistry targeting HCoV-OC43 spike in the nasal passages of IFNAR  $-/-$  mice untreated or treated with IgG or with an anti-IFN $\lambda$ 2 ( $10^7$  FFU dose., day 3 post-infection). (no treatment; n = 3, IgG; n = 5, anti- $\lambda$ ; n = 5)

Scoring was as follows; 0 = no immunoreactivity observed, 1 = rare single cell immunoreactivity, 2 = multifocal small sporadic aggregates of immunoreactive cells.

H&E and corresponding IHC representative images display an increased propensity for spike immunoreactivity in the olfactory epithelium with spike antigen protruding into the respiratory epithelium

(B) Representative pictures of histopathological manifestations (H&E, top) and anti-Spike immunohistochemistry (bottom) of the olfactory (left) and respiratory (right) epithelium of IFNAR  $-/-$  mice at day 3 post-infection following infection with  $10^7$  FFU of HCoV-OC43 and treatment with an anti-IFN $\lambda$ 2.

Sex	STRAIN	VIRUS	Group	DPI	Nasal passage histologic findings	Morphologic diagnosis	Spike IHC	Lung histologic findings	Spike IHC
M	IFNAR -/-	HCoV-OC43	IFNAR -/- 1E7 (infected only)	3 DPI	Mid neutrophilic and mononuclear infiltrate in respiratory epithelium submucosa	Rhinitis, neutrophilic and mononuclear, mild	TBD	NSF	0
M	IFNAR -/-	HCoV-OC43	IFNAR -/- 1E7 (infected only)	3 DPI	NSF	NSF	2 (Olfactory epithelium)	NSF	0
M	IFNAR -/-	HCoV-OC43	IFNAR -/- 1E7 (infected only)	3 DPI	NSF	NSF	2 (Olfactory epithelium)	NSF	0
F	IFNAR -/-	HCoV-OC43	IFNAR -/- 1E7 (IgG1 control,infected)	3 DPI	NSF	NSF	2 (Olfactory epithelium)	NSF	0
F	IFNAR -/-	HCoV-OC43	IFNAR -/- 1E7 (IgG1 control,infected)	3 DPI	NSF	NSF	2 (Olfactory epithelium)	Minimal perivascular and peribronchiolar mononuclear infiltrate	0
M	IFNAR -/-	HCoV-OC43	IFNAR -/- 1E7 (IgG1 control,infected)	3 DPI	NSF	NSF	2 (Olfactory epithelium)-rescan needed	NSF	0
M	IFNAR -/-	HCoV-OC43	IFNAR -/- 1E7 (IgG1 control,infected)	3 DPI	NSF	NSF	2 (Olfactory epithelium)	Minimal perivascular and peribronchiolar mononuclear infiltrate	0
M	IFNAR -/-	HCoV-OC43	IFNAR -/- 1E7 (IgG1 control,infected)	3 DPI	NSF	NSF	2-3 (Olfactory epithelium)	Minimal perivascular and peribronchiolar mononuclear infiltrate	0
M	IFNAR -/-	HCoV-OC43	IFNAR -/- 1E7 (anti-IFN lamda, infected)	3 DPI	Mid neutrophilic and mononuclear infiltrate in respiratory epithelium submucosa	Rhinitis, neutrophilic and mononuclear, mild	3 (Olfactory and respiratory epithelium)	NSF	0
M	IFNAR -/-	HCoV-OC43	IFNAR -/- 1E7 (anti-IFN lamda, infected)	3 DPI	Mid neutrophilic and mononuclear infiltrate in respiratory epithelium submucosa	Rhinitis, neutrophilic and mononuclear, moderate with edema, and ductular degeneration	3 (Olfactory and respiratory epithelium)	NSF	0
M	IFNAR -/-	HCoV-OC43	IFNAR -/- 1E7 (anti-IFN lamda, infected)	3 DPI	Mid neutrophilic and mononuclear infiltrate in respiratory epithelium submucosa	Rhinitis, neutrophilic and mononuclear, mild	2-3 (Olfactory epithelium)	NSF	0
F	IFNAR -/-	HCoV-OC43	IFNAR -/- 1E7 (anti-IFN lamda, infected)	3 DPI	Mid neutrophilic and mononuclear infiltrate in respiratory epithelium submucosa	Rhinitis, neutrophilic and mononuclear, moderate with edema, and ductular degeneration	2 (Olfactory epithelium)	NSF	0
F	IFNAR -/-	HCoV-OC43	IFNAR -/- 1E7 (anti-IFN lamda, infected)	3 DPI	NSF	NSF	TBD	NSF	0
F	IFNAR -/-	HCoV-OC43	IFNAR -/- uninfected	3 DPI	NSF	NSF	0	NSF	0

**Table 14. Histopathology summary of the nasal passages of IFNAR-/- infected with 10<sup>7</sup> FFU of HCoV-OC43.**

Mice were euthanized at day 3 post-infection and treated or not with IgG or with an anti-IFNλ2 (107 FFU dose., day 3 post-infection). (no treatment; n = 3, IgG; n = 5, anti-λ; n = 5)

## DISCUSSION

### **Mice lacking Type-1 Interferon receptor (IFNAR $-/-$ ) display increased susceptibility to HCoV-OC43 infection**

Coronaviruses pose a considerable global threat worldwide. With the potential for additional coronaviruses with pandemic potential to emerge, it is imperative to develop a robust arsenal of countermeasures against these pathogens. Animal models are crucial in this process as they provide platforms to characterize viral pathogenesis and can serve as vaccine efficacy models that are less associated with ethical considerations. While mice stand as ideal platforms for such purposes, they remain refractory to infection by endemic coronaviruses or poorly recapitulate the human disease induced by these viruses. For HCoV-OC43 especially, mouse models developing disease upon infection display severe viral neurotropism and rely on intracranial inoculation routes, which is a far deviation from the natural transmission or exposure route seen in humans. Therefore, there is today a critical unmet need to identify novel mouse models of HCoV-OC43 infection that can foster our understanding of this virus and enable the evaluation of antiviral countermeasures against it. Our goal in this study was to identify and characterize novel mouse models of HCoV-OC43 infection. Using virological and histopathological approaches, our work ultimately shows that type-I and type-III interferon signaling drive the restriction of HCoV-OC43 infection in mice.

Based on our findings, infection of IFNAR  $-/-$  mice is characterized by increased viral replication in the olfactory epithelium compared to C57BL/6 mice. However, viral replication did not extend to the respiratory epithelium and no viral dissemination was

observed. These findings were especially apparent upon the use of a  $10^7$  viral dose, suggesting that other immune barriers may be overcome upon infection with a high viral inoculum.

C57BL/6 wild-type mice showed only a few anti-Spike immunoreactivities in the olfactory epithelium and less frequent histopathology even at a  $10^7$  viral dose.

Our model depicts viral kinetics where the highest level of viral replication in the nasal cavity of IFNAR  $-/-$  mice is reached at 3 days post-infection, prior to viral clearance at 7 days post-infection. While no infectious viral particles were recovered from the lung of both C57BL/6 and IFNAR  $-/-$  mice through the entire infection course, viral RNA could be amplified from the lung of IFNAR  $-/-$  between day 1 and day 7 post-infection and persisted throughout at similar levels. This is in contrast with C57BL/6 mice, which displayed incrementally decreasing viral RNA copies over time in the lung. We conclude that type-I interferon is one major restriction barrier of HCoV-OC43 infection in mice and that there are other barriers likely playing a role in restricting viral dissemination through the respiratory tract.

### **The contribution of type I IFN signaling in restricting HCoV-OC43 infection in mice and governing viral tropism**

Our results provide evidence that type-I IFN signaling restricts HCoV-OC43 infection in the nasal cavity. However, unlike mice, HCoV-OC43 can establish infections in humans in the context of functional type I IFN responses, suggesting an ability of this virus to specifically evade these responses in a human-specific manner.

Consistently, many studies have reported the ability of SARS-CoV-2 evade innate immune response in the early stage of infection, which is an important driver of viral pathogenesis. Many of the proteins encoded in the viral RNA genome of coronaviruses, such as the NSP in HCoV-OC43 and SARS-CoV-2, not only assist with replication but aid in inhibiting host immune responses. An important immune evasion mechanism is preventing the translation of host mRNA for antiviral responses. By inhibiting translation, this results in preventing host antiviral responses [20]. NSP1 in SARS-CoV-2 is a known type-I interferon antagonist and therefore can restrict interferon signaling and production. Additionally, it is highlighted in literature that NSP1 inhibits IRF3 phosphorylation, therefore impairing ISG synthesis. NSP1 can also degrade TYK2, disrupting JAK/STAT signaling and ISG production[99]. Importantly, HCoV-OC43 like SARS-CoV-2 is also Betacoronavirus and could use similar mechanisms to inhibit type I IFN responses in humans. On the contrary, HCoV-OC43 is likely unable to evade some or all of these mechanisms, preventing extensive infection and disease. We can hypothesize that genetic differences between human and mouse effectors of the type I IFN responses may affect the ability for HCoV-OC43 to inhibit or degrade immune mediators in mouse cells. Alternatively, this virus may also encounter an antiviral mechanism not found in humans. A clearer understanding of the mouse-specific mechanisms restricting HCoV-OC43 infection in mice could prove critical to developing mouse models recapitulating human disease upon infection by this virus and that would be amenable for evaluating antiviral countermeasures.

### **The lack of dissemination of HCoV-OC43 in mice suggest the existence of other immunological barriers**

Immunohistochemistry staining depicted little to no spike immunoreactivity in the lungs of IFNAR  $-/-$  mice upon HCoV-OC43 infection, suggesting that other mouse-specific immune barriers may restrict HCoV-OC43 dissemination to the respiratory tract. Type-III IFN signaling has been identified to play a major role in preventing the dissemination of respiratory viruses to the lower respiratory tract. Indeed, mice intranasally treated with IFN- $\lambda$  display increased protection against respiratory viruses such as influenza and SARS-CoV-2. IFNAR  $-/-$  mice challenged with influenza A virus and intranasally administered with IFN- $\lambda$  exhibited reduced viral dissemination to the lungs and lower respiratory tract. The well-established SARS-CoV-2 K18-hACE2 transgenic mouse model also corroborated these findings and showed decreased histopathology in the lungs when treated with IFN- $\lambda$  following SARS-CoV-2 challenge, compared to untreated, infected mice.

Consistent with the literature, we found that IFNAR  $-/-$  mice treated with anti-IFN $\lambda$  displayed increased viral replication in the nasal passages, which is associated with possible dissemination of the virus to the respiratory epithelium.

Therefore, our findings suggest that both type-I and type-III interferon signaling restrict HCoV-OC43 infection in mice and underscore the inability of HCoV-OC43 to overcome these immune barriers in contrast to their human counterpart. However, no Spike immunoreactivity was found in the lung upon anti-IFN $\lambda$  treatment, highlighting that more work is required to evaluate more precisely the contribution of type-III interferon

signaling in restricting HCoV-OC43 dissemination. As our antibody directly targets IFN $\lambda$  and not the type III IFN receptor, this may limit its efficacy in preventing effective type III IFN signaling as IFN $\lambda$  are rapidly and sustainably secreted following infection while a receptor can be effectively saturated prior to viral challenge. The use of mice knock-out for the type III IFN receptor, or of antibody targeting this receptor, should allow to better capture the role of type III IFN signaling in the restriction of HCoV-OC43 infection and dissemination.

### **The potential of IFNAR $-/-$ to serve as platform for testing antiviral countermeasures against HCoV-OC43**

To be suitable for the evaluation of vaccines and therapeutics against viruses, mouse models need to be robustly permissive to viral infection. The ability of mouse models to develop human-like diseases and pathologies upon infection provides another layer of readouts that extend our ability to characterize vaccine and antiviral drug efficacy.

IFNAR  $-/-$  mice inoculated with HCoV-OC43 present certain advantages in evaluating vaccines. Indeed, effective viral in the nasal passages and mild histopathology in the respiratory epithelium of the nasal passages could serve as valuable readouts to evaluate the efficacy of a protective vaccine. However, this model still carries important limitations for such a purpose. When infected, irrespectively of the viral dose, we observed a rapid viral clearance in the nasal passages. This may render challenging to discriminate vaccine-induced viral clearance and host-mediated clearance.

While effective in protecting from severe disease, SARS-CoV-2 vaccines have highlighted the limitations of vaccination approaches against respiratory pathogens in preventing infection. Therefore, a mouse model supporting only infection and not severe disease may not allow to capture the potential efficacy of a vaccine against HCoV-OC43. Furthermore, the lack of viral replication and dissemination in the lung of IFNAR  $-/-$  also limits the potential for vaccine efficacy readouts.

Nevertheless, IFNAR  $-/-$  mice may still be useful to test mucosal or nasal vaccines against HCoV-OC43. IFNAR  $-/-$  mice may also provide insight into whether conventional intramuscular vaccination may restrict viral replication in the nasal cavity – at least for this specific pathogen.

To overcome some of these limitations observed with the IFNAR  $-/-$  mice, the disruption of type-III interferon is a promising path forward. While our observations with IFNAR  $-/-$  mice treated with anti-IFN $\lambda$  displayed elevated levels of spike in the olfactory epithelium with mild protrusions into the respiratory epithelium, a broader and more sustained disruption of the type-III IFN signaling may further enhance permissiveness to HCoV-OC43 infection, making this model more suitable for testing vaccines.

However, it is also worth noting that, disrupting type-I interferon signaling may affect the development of accurate vaccine responses. While the adaptive immune response drives humoral responses and neutralizes antibody production, the innate and adaptive immune compartments congruously work together to induce robust vaccine-induced immune responses. This is particularly exemplified by the live attenuated Yellow Fever 17D vaccine, which is one of the most effective vaccines to date. 17D vaccine can provide

lifetime protection against yellow fever virus. The high efficiency of the vaccine is driven by the induction of both innate and adaptive immune responses upon vaccination, which include the type I IFN response [98]. Therefore, disruption of type I IFN signaling via genetic strategies (e.g., knock-out) could negatively impact the development of vaccine-induced responses and bias vaccine efficacy characterization.

However, antibody treatment targeting type I and/or type III IFN signaling could overcome some of these limitations. Indeed, antibody treatments abrogating IFNAR and/or IFNLR-mediated signaling at the time of infection only, but not at the time of vaccination, could enhance and temporarily render a mouse model permissive to infection without negatively impacting the establishment of effective vaccine-induced immune responses upon vaccination.

Taken together, the development of robust antibody treatment protocols would help with increasing the suitability of IFN signaling-defective mice for evaluating vaccines against HCoV-OC43.

### **Future directions**

Our work is a considerable leap forward in modeling HCoV-OC43 infection in a small animal model. While previous mouse models were refractory to HCoV-OC43 infection in the nasal cavities and respiratory tract, we show for the first time that a mouse model can sustain significant HCoV-OC43 replication in the nasal passages upon disruption of specific antiviral signaling pathways. Through collaborations between several different NEIDL laboratories and industry partners, this thesis delves into the many elements

behind the early-stage development of novel animal models of virus infection. While the mouse model developed during this work does not constitute a comprehensive platform yet to evaluate vaccines and antiviral drugs against HCoV-OC43, our work opens avenues for better understanding the immune barriers restricting HCoV-OC43 replication in mice. Such knowledge will ultimately pave the way for developing refined mouse models that could prove instrumental for evaluating antiviral countermeasures against HCoV-OC43. Especially, investigating how type-III IFN signaling regulates HCoV-OC43 infection and replication (but also other human coronavirus infections) in the mouse respiratory tract appears as a critical step toward better mouse models of HCoV-OC43 infection and disease. The multidisciplinary nature of our study, from histopathology and virology to immunology and animal model development, underscores how the synergy of multiple expertise and scientific concepts can benefit virus research and ultimately, the development of clinical interventions and public health strategies

**BIBLIOGRAPHY**

- [1] Common Human Coronaviruses. Published 2022. Accessed August 23, 2022. <https://www.cdc.gov/coronavirus/general-information.html>
- [2] Coronaviridae. (2012). *Virus Taxonomy*, 806–828. <https://doi.org/10.1016/b978-0-12-384684-6.00068-9>
- [3] Jo, W. K., Drosten, C., & Drexler, J. F. (2021). The evolutionary dynamics of endemic human coronaviruses. *Virus Evolution*, 7(1). <https://doi.org/10.1093/ve/veab020>
- [4] Liu, D. X., Liang, J. Q., & Fung, T. S. (2021). Human Coronavirus-229E, -OC43, -NL63, and -HKU1 (Coronaviridae). *Encyclopedia of Virology*, 428–440. <https://doi.org/10.1016/b978-0-12-809633-8.21501-x>
- [5] Origins of Coronaviruses. (2022, March 16). Nih.gov. <https://www.niaid.nih.gov/diseases-conditions/origins-coronaviruses>
- [6] Huynh, J., Li, S., Yount, B., Smith, A., Sturges, L., Olsen, J. C., Nagel, J., Johnson, J. B., Agnihothram, S., Gates, J. E., Frieman, M. B., Baric, R. S., & Donaldson, E. F. (2012). Evidence Supporting a Zoonotic Origin of Human Coronavirus Strain NL63.
- [7] Fielding, B. C. (2011). Human coronavirus NL63: a clinically important virus? *Future Microbiology*, 6(2), 153–159. <https://doi.org/10.2217/fmb.10.166>
- [8] Esper, F., Weibel, C., Ferguson, D., Landry, M. L., & Kahn, J. S. (2006). Coronavirus HKU1 Infection in the United States. *Emerging Infectious Diseases*, 12(5), 775–779. <https://doi.org/10.3201/eid1205.051316>
- [9] Kesheh, M. M., Hosseini, P., Soltani, S., & Zandi, M. (2021). An overview on the seven pathogenic human coronaviruses. *Reviews in Medical Virology*, 32(2). <https://doi.org/10.1002/rmv.2282>
- [10] Bazant, M. Z., & Bush, J. W. M. (2021). A guideline to limit indoor airborne transmission of COVID-19. *Proceedings of the National Academy of Sciences*, 118(17). <https://doi.org/10.1073/pnas.2018995118>
- [11] Principi, N., Bosis, S., & Esposito, S. (2010). Effects of Coronavirus Infections in Children. *Emerging Infectious Diseases*, 16(2), 183–188. <https://doi.org/10.3201/eid1602.090469>

- [12] Tao, K., Tzou, P. L., Nouhin, J., Gupta, R. K., de Oliveira, T., Kosakovsky Pond, S. L., Fera, D., & Shafer, R. W. (2021). The biological and clinical significance of emerging SARS-CoV-2 variants. *Nature Reviews Genetics*, 22(12), 757–773. <https://doi.org/10.1038/s41576-021-00408-x>
- [13] Miller, I. F., Becker, A. D., Grenfell, B. T., & Metcalf, C. J. E. (2020). Disease and healthcare burden of COVID-19 in the United States. *Nature Medicine*, 26(8), 1212–1217. <https://doi.org/10.1038/s41591-020-0952-y>
- [14] Office. (2023). COVID-19 Vaccines. U.S. Food and Drug Administration. <https://www.fda.gov/emergency-preparedness-and-response/coronavirus-disease-2019-covid-19/covid-19-vaccines>
- [15] Hobbs, E. C., & Reid, T. J. (2020). Animals and SARS - CoV - 2: Species susceptibility and viral transmission in experimental and natural conditions, and the potential implications for community transmission. *Transboundary and Emerging Diseases*, 68(4), 1850–1867. <https://doi.org/10.1111/tbed.13885>
- [16] Anderson, E. M., Goodwin, E. C., Verma, A., Arevalo, C. P., Bolton, M. J., Weirick, M. E., ... Alanio, C. (2020). Seasonal human coronavirus antibodies are boosted upon SARS-CoV-2 infection but not associated with protection. <https://doi.org/10.1101/2020.11.06.20227215>
- [17] Brant, A. C., Tian, W., Majerciak, V., Yang, W., & Zheng, Z.-M. (2021). SARS-CoV-2: from its discovery to genome structure, transcription, and replication. *Cell & Bioscience*, 11(1). <https://doi.org/10.1186/s13578-021-00643-z>
- [18] Human Respiratory Coronavirus OC43: Genetic Stability and Neuroinvasion | *Journal of Virology*. (2023). *Journal of Virology*. <https://journals.asm.org/doi/10.1128/JVI.78.16.8824-8834.2004>
- [19] Jiang, Y., Yin, W., & Xu, H. E. (2021). RNA-dependent RNA polymerase: Structure, mechanism, and drug discovery for COVID-19. *Biochemical and Biophysical Research Communications*, 538, 47–53. <https://doi.org/10.1016/j.bbrc.2020.08.116>
- [20] Zandi, M., Shafaati, M., Kalantar-Neyestanaki, D., Pourghadamyari, H., Fani, M., Soltani, S., Kaleji, H., & Abbasi, S. (2022). The role of SARS-CoV-2 accessory proteins in immune evasion. *Biomedicine & Pharmacotherapy*, 156, 113889. <https://doi.org/10.1016/j.biopha.2022.113889>

- [21] Wang, R., Yang, X., Chang, M., Xue, Z., Wang, W., Bai, L., Zhao, S., & Liu, E. (2021). ORF3a Protein of Severe Acute Respiratory Syndrome Coronavirus 2 Inhibits Interferon-Activated Janus Kinase/Signal Transducer and Activator of Transcription Signaling via Elevating Suppressor of Cytokine Signaling 1. *Frontiers in Microbiology*, 12. <https://doi.org/10.3389/fmicb.2021.752597>
- [22] Hayn, M., Hirschenberger, M., Koepke, L., Nchioua, R., Straub, J. H., Klute, S., Hunszinger, V., Zech, F., Bozzo, C. P., Aftab, W., Christensen, M. H., Conzelmann, C., Müller, J. A., Badarinarayan, S. S., Stürzel, C. M., Forne, I., Stenger, S., Conzelmann, K.-K., Münch, J., & Schmidt, F. I. (2021). Systematic Functional Analysis of SARS-CoV-2 Proteins Uncovers Viral Innate Immune Antagonists and Remaining Vulnerabilities. *Cell Reports*, 109126. <https://doi.org/10.1016/j.celrep.2021.109126>
- [23] Kasuga, Y., Zhu, B., Jang, K.-J., & Yoo, J.-S. (2021). Innate immune sensing of coronavirus and viral evasion strategies. *Experimental & Molecular Medicine*, 53(5), 723–736. <https://doi.org/10.1038/s12276-021-00602-1>
- [24] Mariano, G., Farthing, R. J., Lale-Farjat, S. L. M., & Bergeron, J. R. C. (2020). Structural Characterization of SARS-CoV-2: Where We Are, and Where We Need to Be. *Frontiers in Molecular Biosciences*, 7. <https://doi.org/10.3389/fmolb.2020.605236>
- [25] Vijgen, L., Keyaerts, E., MoësE., Thoelen, I., Wollants, E., Lemey, P., Vandamme, A.-M., & Van Ranst, M. (2005). Complete Genomic Sequence of Human Coronavirus OC43: Molecular Clock Analysis Suggests a Relatively Recent Zoonotic Coronavirus Transmission Event. *Journal of Virology*, 79(3), 1595–1604. <https://doi.org/10.1128/jvi.79.3.1595-1604.2005>
- [26] Li, F. (2016). Structure, Function, and Evolution of Coronavirus Spike Proteins. *Annual Review of Virology*, 3(1), 237–261. <https://doi.org/10.1146/annurev-virology-110615-042301>
- [27] Huang, Y., Yang, C., Xu, X., Xu, W., & Liu, S. (2020). Structural and functional properties of SARS-CoV-2 spike protein: potential antivirus drug development for COVID-19. *Acta Pharmacologica Sinica*, 41(9), 1141–1149. <https://doi.org/10.1038/s41401-020-0485-4>
- [28] Tortorici, M. A., Walls, A. C., Lang, Y., Wang, C., Li, Z., Koerhuis, D., ... Veessler, D. (2019). Structural basis for human coronavirus attachment to sialic acid receptors. *Nature Structural & Molecular Biology*, 26(6), 481–489. <https://doi.org/10.1038/s41594-019-0233-y>

- [29] Burzyńska, P., Sobala, Ł., Mikołajczyk, K., Jodłowska, M., & Jaśkiewicz, E. (2021). Sialic Acids as Receptors for Pathogens. *Biomolecules*, 11(6), 831. <https://doi.org/10.3390/biom11060831>
- [30] Kistler, K. E., & Bedford, T. (2021, January 19). Evidence for adaptive evolution in the receptor-binding domain of seasonal coronaviruses OC43 and 229e. *ELife*; eLife Sciences Publications, Ltd. <https://elifesciences.org/articles/64509>
- [31] IFITM3 interferon induced transmembrane protein 3 [Homo sapiens (human)] - Gene - NCBI. (2023). Retrieved March 7, 2023, from Nih.gov website: <https://www.ncbi.nlm.nih.gov/gene/10410>
- [32] Zhao, X., Li, J., Winkler, C. A., An, P., & Guo, J.-T. (2019). IFITM Genes, Variants, and Their Roles in the Control and Pathogenesis of Viral Infections. *Frontiers in Microbiology*, 9. <https://doi.org/10.3389/fmicb.2018.03228>
- [34] Zhao, X., Guo, F., Liu, F., Cuconati, A., Chang, J., Block, T. M., & Guo, J.-T. (2014). Interferon induction of IFITM proteins promotes infection by human coronavirus OC43. *Proceedings of the National Academy of Sciences*, 111(18), 6756–6761. <https://doi.org/10.1073/pnas.1320856111>
- [35] Schönfelder, K., Breuckmann, K., Elsner, C., Dittmer, U., Fistera, D., Herbstreit, F., Risse, J., Schmidt, K., Sutharsan, S., Taube, C., Jöckel, K.-H., Siffert, W., Kribben, A., & Möhlendick, B. (2021). The influence of IFITM3 polymorphisms on susceptibility to SARS-CoV-2 infection and severity of COVID-19. *Cytokine*, 142, 155492. <https://doi.org/10.1016/j.cyto.2021.155492>
- [36] Crux, N. B., & Elahi, S. (2017). Human Leukocyte Antigen (HLA) and Immune Regulation: How Do Classical and Non-Classical HLA Alleles Modulate Immune Response to Human Immunodeficiency Virus and Hepatitis C Virus Infections? *Frontiers in Immunology*, 8. <https://doi.org/10.3389/fimmu.2017.00832>
- [37] HLA Class I Antigen Serves as a Receptor for Human Coronavirus OC43. (2023). Retrieved March 13, 2023, from Immunological Investigations website: <https://www.tandfonline.com/doi/abs/10.3109/08820139309063393>
- [38] Hidalgo, P., Valdés, M., & González, R. A. (2021). Molecular biology of coronaviruses: an overview of virus-host interactions and pathogenesis. *Boletín Médico Del Hospital Infantil de México*, 78(1). <https://doi.org/10.24875/bmhim.20000249>
- [39] Fehr, A. R., & Perlman, S. (2015). Coronaviruses: An Overview of Their Replication and Pathogenesis. *Coronaviruses*, 1282, 1–23. [https://doi.org/10.1007/978-1-4939-2438-7\\_1](https://doi.org/10.1007/978-1-4939-2438-7_1)

- [40] Sethna, P. B., Hofmann, M. A., & Brian, D. A. (1991). Minus-strand copies of replicating coronavirus mRNAs contain antileaders. *Journal of Virology*, 65(1), 320–325. <https://doi.org/10.1128/jvi.65.1.320-325.1991>
- [41] Pizzato, M., Baraldi, C., Boscato Sopetto, G., Finozzi, D., Gentile, C., Gentile, M. D., Marconi, R., Paladino, D., Raoss, A., Riedmiller, I., Ur Rehman, H., Santini, A., Succetti, V., & Volpini, L. (2022). SARS-CoV-2 and the Host Cell: A Tale of Interactions. *Frontiers in Virology*, 1. <https://doi.org/10.3389/fviro.2021.815388>
- [42] Alberts, B., Johnson, A., Lewis, J., Raff, M., Roberts, K., & Walter, P. (2023). *Innate Immunity*. Nih.gov; Garland Science. <https://www.ncbi.nlm.nih.gov/books/NBK26846/#:~:text=The%20innate%20immune%20responses%20are,present%20in%20the%20uninfected%20host.>
- [43] Heise, M. T. (2014). *Viral Pathogenesis*. Reference Module in Biomedical Sciences. <https://doi.org/10.1016/b978-0-12-801238-3.00079-9>
- [44] El-Zayat, S. R., Sibaii, H., & Mannaa, F. A. (2019). Toll-like receptors activation, signaling, and targeting: an overview. *Bulletin of the National Research Centre*, 43(1). <https://doi.org/10.1186/s42269-019-0227-2>
- [45] Abbas, A. K., Lichtman, A. H., & Pillai, S. (2020). *Basic immunology: Functions and disorders of the immune system* (6th ed.). Elsevier.
- [46] Nilsen, N. J., Vladimer, G. I., Stenvik, J., Orning, M. P. A., Zeid-Kilani, M. V., Bugge, M., Bergstroem, B., Conlon, J., Husebye, H., Hise, A. G., Fitzgerald, K. A., Espevik, T., & Lien, E. (2015). A Role for the Adaptor Proteins TRAM and TRIF in Toll-like Receptor 2 Signaling. *Journal of Biological Chemistry*, 290(6), 3209–3222. <https://doi.org/10.1074/jbc.m114.593426>
- [47] Rehwinkel, J., & Gack, M. U. (2020). RIG-I-like receptors: their regulation and roles in RNA sensing. *Nature Reviews Immunology*, 20(9), 537–551. <https://doi.org/10.1038/s41577-020-0288-3>
- [48] Loo, Y.-M., & Gale, M. (2011). Immune Signaling by RIG-I-like Receptors. *Immunity*, 34(5), 680–692. <https://doi.org/10.1016/j.immuni.2011.05.003>
- [49] Zhou, R., Zhang, Q., & Xu, P. (2020). TBK1, a central kinase in innate immune sensing of nucleic acids and beyond. *Acta Biochimica et Biophysica Sinica*, 52(7), 757–767. <https://doi.org/10.1093/abbs/gmaa051>

- [50] Petes, C., Odoardi, N., & Gee, K. (2017). The Toll for Trafficking: Toll-Like Receptor 7 Delivery to the Endosome. *Frontiers in Immunology*, 8. <https://doi.org/10.3389/fimmu.2017.01075>
- [51] Farooq, M., Batool, M., Kim, M. S., & Choi, S. (2021). Toll-Like Receptors as a Therapeutic Target in the Era of Immunotherapies. *Frontiers in Cell and Developmental Biology*, 9. <https://doi.org/10.3389/fcell.2021.756315>
- [52] Hagel, K. (2018, July 9). An introduction to interferons. Retrieved March 7, 2023, from ImmunoBites website: <https://immunobites.com/2018/07/09/an-introduction-to-interferons/>
- [53] Fitzgerald-Bocarsly, P., & Feng, D. (2007). The role of type I interferon production by dendritic cells in host defense. *Biochimie*, 89(6-7), 843–855. <https://doi.org/10.1016/j.biochi.2007.04.018>
- [54] Antigen-Presenting Cells. (2012). *Immunology for Pharmacy*, 37–44. <https://doi.org/10.1016/b978-0-323-06947-2.10005-7>
- [55] McKenna, K., Beignon, A.-S. ., & Bhardwaj, N. (2004). Plasmacytoid Dendritic Cells: Linking Innate and Adaptive Immunity. *Journal of Virology*, 79(1), 17–27. <https://doi.org/10.1128/jvi.79.1.17-27.2005>
- [56] Chauhan, D., Singh, A. V., Brahmandam, M., Carrasco, R., Bandi, M., Hideshima, T., Bianchi, G., Podar, K., Tai, Y.-T., Mitsiades, C., Raje, N., Jaye, D. L., Kumar, S. K., Richardson, P., Munshi, N., & Anderson, K. C. (2009). Functional Interaction of Plasmacytoid Dendritic Cells with Multiple Myeloma Cells: A Therapeutic Target. *Cancer Cell*, 16(4), 309–323. <https://doi.org/10.1016/j.ccr.2009.08.019>
- [57] Le Bon, A., & Tough, D. F. (2002). Links between innate and adaptive immunity via type I interferon. *Current Opinion in Immunology*, 14(4), 432–436. [https://doi.org/10.1016/s0952-7915\(02\)00354-0](https://doi.org/10.1016/s0952-7915(02)00354-0)
- [58] Kim, Y.-M., & Shin, E.-C. (2021). Type I and III interferon responses in SARS-CoV-2 infection. *Experimental & Molecular Medicine*, 53(5), 750–760. <https://doi.org/10.1038/s12276-021-00592-0>
- [59] Zanin, N., Viaris de Lesegno, C., Lamaze, C., & Blouin, C. M. (2021). Interferon Receptor Trafficking and Signaling: Journey to the Cross Roads. *Frontiers in Immunology*, 11. <https://doi.org/10.3389/fimmu.2020.615603>

- [60] Domizio, J. D., Gulen, M. F., Saidoune, F., Thacker, V. V., Yatim, A., Sharma, K., ... Ablasser, A. (2022). The cGAS–STING pathway drives type I IFN immunopathology in COVID-19. *Nature*, 603(7899), 145–151. <https://doi.org/10.1038/s41586-022-04421-w>
- [61] Wack, A., Terczyńska-Dyla, E., & Hartmann, R. (2015). Guarding the frontiers: the biology of type III interferons. *Nature Immunology*, 16(8), 802–809. <https://doi.org/10.1038/ni.3212>
- [62] Stanifer, M. L., Pervolaraki, K., & Boulant, S. (2019). Differential Regulation of Type I and Type III Interferon Signaling. *International Journal of Molecular Sciences*, 20(6), 1445. <https://doi.org/10.3390/ijms20061445>
- [63] Stanifer, M. L., Guo, C., Doldan, P., & Boulant, S. (2020). Importance of Type I and III Interferons at Respiratory and Intestinal Barrier Surfaces. *Frontiers in Immunology*, 11. <https://doi.org/10.3389/fimmu.2020.608645>
- [64] Hemann, E. A., Gale, M., & Savan, R. (2017). Interferon Lambda Genetics and Biology in Regulation of Viral Control. *Frontiers in Immunology*, 8. <https://doi.org/10.3389/fimmu.2017.01707>
- [65] Lazear, H. M., Schoggins, J. W., & Diamond, M. S. (2019). Shared and Distinct Functions of Type I and Type III Interferons. *Immunity*, 50(4), 907–923. <https://doi.org/10.1016/j.immuni.2019.03.025>
- [66] Forero, A., Ozarkar, S., Li, H., Lee, C. H., Hemann, E. A., Nadjisombati, M. S., Hendricks, M. R., So, L., Green, R., Roy, C. N., Sarkar, S. N., von Moltke, J., Anderson, S. K., Gale, M., & Savan, R. (2019). Differential Activation of the Transcription Factor IRF1 Underlies the Distinct Immune Responses Elicited by Type I and Type III Interferons. *Immunity*, 51(3), 451-464.e6. <https://doi.org/10.1016/j.immuni.2019.07.007>
- [67] Hermant, P., & Michiels, T. (2014). Interferon- $\lambda$  in the Context of Viral Infections: Production, Response and Therapeutic Implications. *Journal of Innate Immunity*, 6(5), 563–574. <https://doi.org/10.1159/000360084>
- [68] Chong, Z., Karl, C. E., Halfmann, P. J., Kawaoka, Y., Winkler, E. S., Yu, J., & Diamond, M. S. (2022). Nasally-delivered interferon- $\lambda$  protects mice against upper and lower respiratory tract infection of SARS-CoV-2 variants including Omicron. <https://doi.org/10.1101/2022.01.21.477296>

- [69] Bertram, S., Dijkman, R., Habjan, M., Heurich, A., Gierer, S., Glowacka, I., ... Pöhlmann, S. (2013). TMPRSS2 Activates the Human Coronavirus 229E for Cathepsin-Independent Host Cell Entry and Is Expressed in Viral Target Cells in the Respiratory Epithelium. *Journal of Virology*, 87(11), 6150–6160. <https://doi.org/10.1128/jvi.03372-12>
- [70] Schoeman, D., Gordon, B., & Fielding, B. C. (2021). Pathogenic Human Coronaviruses. Reference Module in Biomedical Sciences. <https://doi.org/10.1016/B978-0-12-818731-9.00052-5>
- [71] Konopka, K. E., Nguyen, T., Jentzen, J. M., Rayes, O., Schmidt, C. J., Wilson, A. M., Farver, C. F., & Myers, J. L. (2020). Diffuse alveolar damage (DAD) resulting from coronavirus disease 2019 Infection is Morphologically Indistinguishable from Other Causes of DAD. *Histopathology*, 77(4), 570–578. <https://doi.org/10.1111/his.14180>
- [72] Morgello, S. (2020). Coronaviruses and the central nervous system. *Journal of NeuroVirology*, 26(4), 459–473. <https://doi.org/10.1007/s13365-020-00868-7>
- [73] Chong, Z., Karl, C. E., Halfmann, P. J., Kawaoka, Y., Winkler, E. S., Yu, J., & Diamond, M. S. (2022). Nasally-delivered interferon- $\lambda$  protects mice against upper and lower respiratory tract infection of SARS-CoV-2 variants including Omicron. <https://doi.org/10.1101/2022.01.21.477296>
- [75] Ghimire, D., Han, Y., & Lu, M. (2022). Structural Plasticity and Immune Evasion of SARS-CoV-2 Spike Variants. *Viruses*, 14(6), 1255. <https://doi.org/10.3390/v14061255>
- [76] Khandker, S. S., Godman, B., Jawad, Md. I., Meghla, B. A., Tisha, T. A., Khondoker, M. U., ... Adnan, N. (2021). A Systematic Review on COVID-19 Vaccine Strategies, Their Effectiveness, and Issues. *Vaccines*, 9(12), 1387. <https://doi.org/10.3390/vaccines9121387>
- [77] Li, Y.-D., Chi, W.-Y., Su, J.-H., Ferrall, L., Hung, C.-F., & Wu, T.-C. . (2020). Coronavirus vaccine development: from SARS and MERS to COVID-19. *Journal of Biomedical Science*, 27(1). <https://doi.org/10.1186/s12929-020-00695-2>
- [78] CDC. (2020, February 11). Overview of COVID-19 Vaccines. Centers for Disease Control and Prevention. [https://www.cdc.gov/coronavirus/2019-ncov/vaccines/different-vaccines/overview-COVID-19-vaccines.html?s\\_cid=11758:covid%20vaccine%20brands:sem.ga:p:RG:GM:gen:PTN:FY22](https://www.cdc.gov/coronavirus/2019-ncov/vaccines/different-vaccines/overview-COVID-19-vaccines.html?s_cid=11758:covid%20vaccine%20brands:sem.ga:p:RG:GM:gen:PTN:FY22)

- [79] Burki, T. (2020). The online anti-vaccine movement in the age of COVID-19. *The Lancet Digital Health*, 2(10), e504–e505. [https://doi.org/10.1016/s2589-7500\(20\)30227-2](https://doi.org/10.1016/s2589-7500(20)30227-2)
- [80] Yap, C., Ali, A., Prabhakar, A., Prabhakar, A., Pal, A., Lim, Y. Y., & Kakodkar, P. (2021). Comprehensive literature review on COVID-19 vaccines and role of SARS-CoV-2 variants in the pandemic. *Therapeutic Advances in Vaccines and Immunotherapy*, 9, 251513552110597. <https://doi.org/10.1177/25151355211059791>
- [81] Chen, S., Guan, F., Candotti, F., Benlagha, K., Camara, N. O. S., Herrada, A. A., ... Liu, C. (2022). The role of B cells in COVID-19 infection and vaccination. *Frontiers in Immunology*, 13. <https://doi.org/10.3389/fimmu.2022.988536>
- [83] Kamboj, M., & Sepkowitz, K. (2007). Risk of Transmission Associated With Live Attenuated Vaccines Given to Healthy Persons Caring for or Residing With an Immunocompromised Patient. *Infection Control & Hospital Epidemiology*, 28(6), 702-707. doi:10.1086/517952
- [83] Santacroce, L., Charitos, I. A., Carretta, D. M., De Nitto, E., & Lovero, R. (2020). The human coronaviruses (HCoVs) and the molecular mechanisms of SARS-CoV-2 infection. *Journal of Molecular Medicine*, 99(1), 93–106. <https://doi.org/10.1007/s00109-020-02012-8>
- [84] Bergmann, C. C., & Silverman, R. H. (2020). COVID-19: Coronavirus replication, pathogenesis, and therapeutic strategies. *Cleveland Clinic Journal of Medicine*, 87(6). <https://doi.org/10.3949/ccjm.87a.20047>
- [85] CDC. (2022, November 9). RSV (Respiratory Syncytial Virus). Retrieved March 14, 2023, from Centers for Disease Control and Prevention website: <https://www.cdc.gov/rsv/index.html>
- [86] Sacco, R. E., Durbin, R. K., & Durbin, J. E. (2015). Animal models of respiratory syncytial virus infection and disease. *Current Opinion in Virology*, 13, 117–122. <https://doi.org/10.1016/j.coviro.2015.06.003>
- [87] Okabayashi, T., Kojima, T., Masaki, T., Yokota, S., Imaizumi, T., Tsutsumi, H., Himi, T., Fujii, N., & Sawada, N. (2011). Type-III interferon, not type-I, is the predominant interferon induced by respiratory viruses in nasal epithelial cells. *Virus Research*, 160(1-2), 360–366. <https://doi.org/10.1016/j.virusres.2011.07.011>

- [88] Cilloniz, C., Pantin-Jackwood, M. J., Ni, C., Carter, V. S., Korth, M. J., Swayne, D. E., Tumpey, T. M., & Katze, M. G. (2012). Molecular Signatures Associated with Mx1-Mediated Resistance to Highly Pathogenic Influenza Virus Infection: Mechanisms of Survival. *Journal of Virology*, 86(5), 2437–2446. <https://doi.org/10.1128/jvi.06156-11>
- [89] Verhelst, J., Parthoens, E., Schepens, B., Fiers, W., & Saelens, X. (2012). Interferon-Inducible Protein Mx1 Inhibits Influenza Virus by Interfering with Functional Viral Ribonucleoprotein Complex Assembly. *Journal of Virology*, 86(24), 13445–13455. <https://doi.org/10.1128/jvi.01682-12>
- [90] Mordstein, M., Kochs, G., Dumoutier, L., Renauld, J.-C., Paludan, S. R., Klucher, K., & Staeheli, P. (2008). 267 Interferon- $\lambda$  contributes to innate immunity of mice against influenza A virus but not against hepatotropic viruses. *Cytokine*, 43(3), 307. <https://doi.org/10.1016/j.cyto.2008.07.349>
- [91] Krammer, S., Sicorschi Gutu, C., Grund, J. C., Chiriac, M. T., Zirlik, S., & Finotto, S. (2021). Regulation and Function of Interferon-Lambda (IFN $\lambda$ ) and Its Receptor in Asthma. *Frontiers in Immunology*, 12. <https://doi.org/10.3389/fimmu.2021.731807>
- [92] BALB/c Mice | Charles River. (2023). Retrieved March 9, 2023, from Criver.com website: <https://www.criver.com/products-services/find-model/balbc-mouse?region=3611>
- [93] Jacomy, H., Fragoso, G., Almazan, G., Mushynski, W. E., & Talbot, P. J. (2006). Human coronavirus OC43 infection induces chronic encephalitis leading to disabilities in BALB/C mice. *Virology*, 349(2), 335–346. <https://doi.org/10.1016/j.virol.2006.01.049>
- [94] Niu, J., Shen, L., Huang, B., Ye, F., Zhao, L., Wang, H., ... Tan, W. (2020). Non-invasive bioluminescence imaging of HCoV-OC43 infection and therapy in the central nervous system of live mice. *Antiviral Research*, 173, 104646. <https://doi.org/10.1016/j.antiviral.2019.104646>
- [95] J028288 - Ifnar1[-] Strain Details. (2023). Jax.org. <https://www.jax.org/strain/028288>.
- [96] Welsch, J. C., Charvet, B., Dussurgey, S., Allatif, O., Aurine, N., Horvat, B., Gerlier, D., & Mathieu, C. (2019). Type I Interferon Receptor Signaling Drives Selective Permissiveness of Astrocytes and Microglia to Measles Virus during Brain Infection. *Journal of Virology*, 93(13). <https://doi.org/10.1128/jvi.00618-19>
- [97] Kim MI, Lee C. Human Coronavirus OC43 as a Low-Risk Model to Study COVID-19. *Viruses*. 2023; 15(2):578. <https://doi.org/10.3390/v1502057>

- [98] Querec, T. D., Akondy, R. S., Lee, E. K., Cao, W., Nakaya, H. I., Teuwen, D., Pirani, A., Gernert, K., Deng, J., Marzolf, B., Kennedy, K., Wu, H., Bennouna, S., Oluoch, H., Miller, J., Vencio, R. Z., Mulligan, M., Aderem, A., Ahmed, R., & Pulendran, B. (2008). Systems biology approach predicts immunogenicity of the yellow fever vaccine in humans. *Nature Immunology*, 10(1), 116–125. <https://doi.org/10.1038/ni.1688>
- [99] Yuan, S., Balaji, S., Lomakin, I. B., & Xiong, Y. (2021). Coronavirus Nsp1: Immune Response Suppression and Protein Expression Inhibition. *Frontiers in Microbiology*, 12. <https://doi.org/10.3389/fmicb.2021.752214>

**CURRICULUM VITAE**

